

Hadronization Model Approach from Strongly Coupled QGP in RHIC

Hong Miao¹, Chongshou Gao², Pengfei Zhuang¹

¹*Physics Department, Tsinghua University, Beijing 100084, China and*

²*School of Physics, Peking University, Beijing 100871, China*

A hadron transport method is developed to describe the detailed phase transition which may take place in the relativistic heavy ion collisions. Consequently, a self-consistent hydro-decoupling condition could be deduced, which will put additional boundary conditions into the decoupling hyper surface of the fluid. By solving the hydrodynamic evolution of this type of medium with low viscosity and solving the transport process, the soft hadron production can be well described. As a preliminary application, mid-rapidity transverse momentum spectrum of mesons, baryons and some resonance states in central events are calculated. Most of them are consistent with the RHIC data except $\Sigma^*(1385)$, $\Xi^*(1530)$ and $\phi(1020)$. HBT radii can also be extracted from this model. Considering the decay contribution of the large abundance of resonances emitted and scattering loss in transporting through them, HBT radii will be corrected from those of the direct emitted hadrons. It may provide a possible solution to repeat the HBT data observed in $\pi\pi$ correlations even in hydrodynamic models with large transverse flow.

Key Words: *QGP, Non-equilibrium, Transport, Hadronization, Hydrodynamics*

PACS numbers: 12.38.Mh, 25.75.-q

I. INTRODUCTION

The hot and dense matter created in the relativistic heavy ion collisions is the proper object to investigate the QCD phase structures such as Quark Gluon Plasma (QGP) [1, 2, 3, 4, 5]. Studying the evolution of this expanding fireball and the emission of hadrons which also depends on the details of the hadronization process will benefit our knowledge in this area. In fact, hydrodynamics [6][7][8] based on the condition of local thermal and chemical equilibrium, EOS (Equation of State) of mixed phases and low viscosity, models of quark coalescence [9][10] or recombination [11][12] and fragmentation [13][14] worked quite well to describe most parts of the RHIC data in deferent p_T regions. While other questions also remind us: how about the non-equilibrium fireball works? Considering that the finite size [15] created in the impact, the large fluctuations and the small duration it evolves or cools as reported in HBT measurements [16], such possibility should not be neglected [17]. Discussions based on these conditions will be helpful for us to establish a better understanding on this problem, to confirm the rationality of some of widely used methods or even to extent some of them.

Firstly, it is noticed that the initial formation time τ_0 for the thermal equilibrium of quark matter is regarded to be $0.4 - 0.6 fm/c$ in RHIC [18][4]. But the formation time for hadronic matter which is far less in energy density would be much longer as $\tau_0 \geq 1 fm/c$. That means when the ideal QGP fluid is formed and starts to evolve under hydrodynamics, the surrounded hadronic gas is far from equilibrium. In this situation, a system with complete local thermal and chemical equilibrium, such as the mixed phase which usually exists in an infinite thermal system, is hardly to be established. It is more likely to be an expanding or shrinking source emitting hadrons to

a kind of rarefied medium or vacuum. Because of the absence of the thermalized mix phases, the evolution will be a little faster.

In this article, a microscopic effective hadronization mechanism, which may be consistent to some of statistical or recombination models, is provided to estimate the "soft" production in the relativistic heavy ion collisions, in which the hadrons would be created in the plasma and emit from the QGP source by an approximate classical transport process. The hadron creation is estimated by an effective tree level universal calculation [19], in which only two coupling constants are used separately for mesons and baryons. The transport will result in a kind of "Evaporation". Evaporation models [20][21][22] developed many years ago were widely used to describe the properties of QGP. A remarkable property of the evaporation models is the emission rate, which is characterized by different models. In some of the models, a simple assumption was used, that the particle emission and absorption balance each other of QGP and Hadronic gas in an infinite system at the critical temperature T_c , which deduces the relations of emission distributions,

$$f_i(\mathbf{p}) = f_{Ti}(\mathbf{p}),$$

where f_{Ti} is the ideal thermal distribution of the relative particles in the hadronic gas. It is noticed that this condition is a little stronger. In fact, only the whole equilibrium for both sides is needed, as the chemical and thermal equilibrium exist in them,

$$\begin{aligned} \sum_i \int v_{ix} f_i(p_i) E_i d\mathbf{p}_i &= \sum_i \int v_{ix} f_{Ti}(p_i) E_i d\mathbf{p}_i, \\ \sum_i \int v_{ix} f_i(p_i) p_{ix} d\mathbf{p}_i &= \sum_i \int v_{ix} f_{Ti}(p_i) p_{ix} d\mathbf{p}_i, \\ \sum_i \int v_{ix} f_i(p_i) n_{ij} d\mathbf{p}_i &= \sum_i \int v_{ix} f_{Ti}(p_i) n_{ij} d\mathbf{p}_i, \end{aligned} \quad (1)$$

where n_{ij} refers to the baryon number, strange number, etc. If only thermal equilibrium is established, another condition should be added,

$$\int v_{ix} f_i(p_i) d\mathbf{p}_i = \int v_{ix} f_{Ti}(p_i) d\mathbf{p}_i.$$

Eqs. (1) will be used in our calculations as necessary conditions in the parameter selections (e.g. coupling constants).

Secondly, due to recent calculations [23][24][25][26], QGP in low temperature regions as $T \sim 1 - 3T_c$ contains large interactions. It is supposed that bound states or resonance states such as diquarks may exist in such kind of Strongly Coupled Quark Gluon Plasma (SQGP). Thus, the production of hadrons in SQGP could be described as quark with anti-quark combining to mesons and quark with diquark combining to baryons.

Considering the finite evaporation rate in the boundaries, the evolution of the system will not only depend on the hydrodynamics expansion, but also depend on the evaporation. When the expansion is small, the hadronization is dominated by the a minimum evaporation rate described in Sec (II C). If the expansion is large, the fluid will be more likely to split to macroscopic structures as bubbles, sponges, fragments and droplets or globes. (Note that even evaporation itself can also produce droplets in microscopic scales.) The fragments and droplets can still interact or be coupled each other by emitting and absorbing hadrons, until they dissociate before a decouple limit is reached. Thus, the fluid can still evolve after the QGP breaks. Large transverse momentum can be produced in this duration.

It is noticed that when QGP source split to small droplets, the interactions of exchanging hadrons between the droplets will be much weaker than the interactions in SQGP. Although there are calculations showing low viscosity in SQGP [27][28], the scenario of droplet interaction would provide another possible mechanism to reduce the viscosity in the fluid, despite of the interactions in the plasma. Such mechanism makes it accessible for the ideal hydrodynamics to work as reported in RHIC [29].

Additionally, considering that the QGP and hadron phases would not be coupled together significantly during the hydrodynamic evolution, the stability of the calculations will benefit from the whole TN (thermodynamically normal) matter [30]. The influence of the inner sonic waves may be minimized.

The calculations are based on a kind of ideal situation contrasting to statistical models. *The SQGP fluid evolves under hydrodynamics, and the hadrons are created by detailed SQGP production process and classical transport.* While, parton distributions are still assumed to be thermalized in this stage. Hadron re-scattering is also neglected from the calculations. That means, only soft productions, where the partons will lose their memories of momentum and energy after each impact, could be estimated. It is supposed that jet partons may cast their

influence on high p_T spectrum of light partons more significantly than the heavy multi-strange baryons (except J/Ψ). Accordingly, re-scattering effects may be more important for low p_T strange baryon resonances, inverse to their strange numbers. Generally, the hadronization process is a complicated issue, in which large amount of effects are involved or coupled together. The main idea to resolve it is to find some operations which can orthonormalize some of these effects and calculate them separately.

The efforts and the attempts to apply it prospectively, are presented in the sections below. In Section (II), the models of hadron production and transport will be discussed, which may deduce an approximate emission distribution. Details of the calculation will be shown in the appendixes. In Section (III), a brief introduction of hydrodynamics, where the fluid will break into droplets near the surface, with effective evaporation boundary conditions in central events will be provided. In Section (IV), RHIC spectra as applications will be discussed. Summaries and outlooks of this model will be presented in Section (V).

II. EMISSION FROM THE SURFACE

Considering that plenty of components would involve together, it is a rough task to develop detailed quantum transport diagrams. Relativistic classical transport theory is used in the calculations. In our models, transport is only used for hadrons. Gluons, quarks, q-g bound states and diquarks are supposed under ideal gas distributions as they may contain more stronger interactions so far. The difference of diquark distribution is considered to be absorbed to the quark-diquark-baryon coupling constants in the calculations.

It should be noted that there are limitations of the classical transport. One of them is that the distribution, regarding $\hbar \rightarrow 0$, breaks the uncertainty relationship. Another one is about the particle volume or wave function. That is, the particle distribution will not only be associated with the environment near the mass center, but also be coupled to the whole phase space. Fluctuations also make troubles for the distributions and transports. Additionally, fluctuations could cause the fluid breaking into pieces, especially in beam direction, although the influence may be limited for mid rapidity productions.

These are fundamental problems of the classical transport. But the detailed interactions between partons and hadrons are not clear, especially for the elastic and inelastic scattering by different partons and hadrons, which are all coupled together. It is not easy to deal with all of these and what can we do is only assume that the classical transport could work in RHIC conditions.

A. Medium Absorption of the Color Singlets

Only the absorption caused by the partons is considered here. The hadronic interaction is neglected for the small relative abundance. Their particle independent effects can be added to the mean cross sections. Considering that tens of hadrons will be discussed, calculations of all of the diagrams on different processes would be quite complicated. Thus, the cross sections here are simplified. The inelastic absorption by parton i is described as

$$\begin{aligned} a_{D0i}(\mathbf{p}) &= f(\mathbf{p}) \int g_i(\mathbf{q}) |\mathbf{v} - \mathbf{v}_q| \sigma_i(\mathbf{p}, \mathbf{q}) d^3\mathbf{q} \\ &= 4\pi f(\mathbf{p}) \int dq g_i(q) q^2 \sigma_i(\mathbf{p}, \mathbf{q}) \\ &\quad \times \frac{(v + v_q)^3 - |v - v_q|^3}{6vv_q}, \end{aligned} \quad (2)$$

where f and g_i correspond to the hadron and parton distributions, $\sigma_i(p, q)$ is the effective cross section. Averaging $\sigma_i(p, q)$ as σ_i , one gets

$$a_{D0}(\mathbf{p}) = f(\mathbf{p})\beta(p) = 4\pi f(\mathbf{p}) \sum_i \sigma_i \zeta_i(p), \quad (3)$$

where,

$$\begin{aligned} \zeta_i(p) &= v \int_0^{\frac{m_i v}{\sqrt{1-v^2}}} g_i(q) q^2 dq + \frac{1}{3v} \int_0^{\frac{m_i v}{\sqrt{1-v^2}}} g_i(q) \frac{q^4}{E_i^2} dq \\ &\quad + \int_{\frac{m_i v}{\sqrt{1-v^2}}}^\infty g_i(q) \frac{q^3}{E_i} dq + \frac{v^2}{3} \int_{\frac{m_i v}{\sqrt{1-v^2}}}^\infty g_i(q) q E_i dq, \end{aligned}$$

with $v = p/E$.

For large p jets passing cold matter,

$$\begin{aligned} \zeta_{iJet(p)} &\approx v \int_0^\infty g_i(q) q^2 dq + \frac{1}{3v} \int_0^\infty g_i(q) \frac{q^4}{E_i^2} dq \\ &= \frac{n_i}{4\pi} [v + \frac{1}{3v} \langle v_i^2 \rangle], \end{aligned} \quad (4)$$

where, $\langle v_i^2 \rangle$ is constant at given temperature and chemical potential. Approximately,

$$a_{D0}(\mathbf{p}) \approx \frac{f(\mathbf{p}, \mathbf{r})v}{L_{in}}, \quad (5)$$

where,

$$L_{in} = \frac{1}{\sum_i n_i \sigma_i}, \quad (6)$$

is the inelastic "free path" and regarded as a consequence of the adjustable parameter $\langle \sigma_m \rangle$ in later sections. The baryon cross section is set to be 1.5 times of the meson cross section, $\langle \sigma_b \rangle = 1.5 \langle \sigma_m \rangle$, due to the valence quark numbers.

For soft distribution in hot medium,

$$\begin{aligned} \zeta_{iEva}(p) &\approx \int_0^\infty g_i(q) \frac{q^3}{E_i} dq + \frac{v^2}{3} \int_0^\infty g_i(q) q E_i dq \\ &= \frac{n_i}{4\pi} [\langle v_i \rangle + \frac{v^2}{3} \langle \frac{1}{v_i} \rangle]. \end{aligned} \quad (7)$$

If light quarks or gluons is considered, $\langle v_i \rangle = \langle \frac{1}{v_i} \rangle = 1$. For strange quarks, $\langle v_i \rangle \approx 0.96$ and $\langle \frac{1}{v_i} \rangle \approx 1.05$, when $m_s = 95 \text{ MeV}$. For simplification, one has,

$$a_{D0}(\mathbf{p}) \approx \frac{1 + v^2/3}{L_{in}} f(\mathbf{p}, \mathbf{r}). \quad (8)$$

B. Transport Near the Boundary

First of all, a most simple stable condition is discussed in this step. Effects of fragments, surface shrinking and hydrodynamics will be presented in Sec (II C) and Sec (III). Here, QGP with fixed energy density ε_b is supposed in $x > 0$ region and the other side is vacuum. The relativistic Boltzmann Equation is,

$$\frac{\partial f}{\partial t} + \mathbf{v} \cdot \nabla f = Q_{rel}(f) + a_p - a_D, \quad (9)$$

where a_p is the production rate, a_D is the loss rate, and

$$\begin{aligned} Q_{rel}(f_i) &= \sum_j \int d\Omega d^3\mathbf{q} \mathcal{K}_c(\mathbf{p}, \mathbf{q}, \Omega) \\ &\quad \times [f_i(\mathbf{p}') f_j(\mathbf{q}') - f_i(\mathbf{p}) f_j(\mathbf{q})], \end{aligned} \quad (10)$$

is the elastic exchange term. Details of \mathbf{q}' , \mathbf{p}' and $\mathcal{K}_c(\mathbf{p}, \mathbf{q}, \Omega)$ can be found in [31].

Generally the solution involves in time evolution are complicated [32]. As the quasi-static condition is supposed, the first term can be temporarily removed from Eq. (9). To deal with the elastic exchange term, which makes tens or hundreds of equations coupled together, relaxation time approximation is used for simplification,

$$\frac{p \cos \theta}{E} \frac{\partial f}{\partial x} = \frac{f - f_T}{\tau_{lax}} + a_p - \beta f, \quad (11)$$

The relaxation time is supposed to be $\tau_{lax} \sim 1 - \infty fm/c$. Generally, τ_{lax} should be different for each hadron in different momentum regions. While, we set it as a universal parameter as a simplification for the global model.

It is noted, the excluded volume of hadrons and resonances may cause a reduction to the phase space and suppress the distributions against the ideal gas distributions [33][34],

$$f_T(p) = (1 - y_{op}) f_{T0}(p),$$

where y_{op} is the occupation ratio of excluded particles. The excluded volume prevents the total particle abundance from exceeding a certain limit, when more resonance states are introduced.

Thus, the solution of Eq. (9) is written as

$$\begin{aligned} f(x, p, \theta) &= \frac{a_p(p) \tau_{lax} + f_T(p)}{\beta(p) \tau_{lax} + 1} \\ &\quad \times \left[1 \pm C(p, \theta) e^{-\frac{\beta(p) \tau_{lax} + 1}{v \tau_{lax} \cos \theta} x} \right] \\ &= f_\infty \left[1 - \left[1 - \frac{f(x_0, p, \theta)}{f_\infty} \right] e^{-\frac{\beta(p) \tau_{lax} + 1}{v \tau_{lax} \cos \theta} (x - x_0)} \right], \end{aligned} \quad (12)$$

where,

$$f_\infty = f(\infty, p, \theta) = \frac{a_p(p)\tau_{lax} + f_T(p)}{\beta(p)\tau_{lax} + 1}. \quad (13)$$

When the hadron decay during the transport process is considered, a_p and a_D are described as,

$$\begin{aligned} a_p &= a_{p0} + a_{pv}, \\ a_D &= a_{D0} + a_{Dv}, \end{aligned}$$

where a_{p0} is the QGP production rate [35][23], which will be discussed in Sec (II D) and a_{D0} is the partonic absorption defined in Eq. (3) or Eq. (8). Hadronic re-scattering is neglected. a_{pv} and a_{Dv} are the spontaneous decay corrections with width Γ and decay contribution F_D [36],

$$a_{pv_i} = \sum_j \int_{\mathbf{p}'} d\mathbf{p}' f_j(\mathbf{p}') \frac{\Gamma_j}{\gamma_j} F_{D_{ji}}(\mathbf{p}', \mathbf{p}_i), \quad (14)$$

$$a_{Dv_i} = \frac{\Gamma_i}{\gamma_i} f_i. \quad (15)$$

Eq. (14) makes the Transport Equation (9) of different components coupled again, especially for the baryon to meson channels, where the absorption cross sections are significantly different. However, if the system is regarded as a steady object, there is a simple solution to decouple them. Term (14) could be pulled out from Eq. (12) to get the suppressed direct production by decay loss and be added to the final decay corrections (41) as a factor $\alpha_{i,j}$ to F_D ,

$$\begin{aligned} \alpha_{i,j} &= 1 + \xi_{j+1,j} \alpha_{i,j+1} \\ &= 1 + \xi_{j+1,j} + \xi_{j+1,j} \xi_{j+2,j+1} + \dots + \xi_{j+1,j} \dots \xi_{i,i-1}, \end{aligned} \quad (16)$$

for each decay series $j, j+1, \dots, i-1, i$. Where,

$$\xi_{j+1,j} = \frac{\langle \eta^{-1} \rangle \frac{\Gamma_j}{\gamma_j}}{[\beta_i + \langle \eta^{-1} \rangle \frac{\Gamma_i}{\gamma_i}] + \tau_{lax}^{-1}}. \quad (17)$$

Here, $\langle \eta^{-1} \rangle$ is a kind of average on QGP droplets occupation η , which will be discussed in Sec (II C) and could be deduced approximately from Eq. (30). For current conditions, $\langle \eta^{-1} \rangle = 1$. Due to Eq. (14) and (16), the life time is no longer the limitation for hadron selections. The selection should be based on mass, components and scattering matrix. It brings a serious problem for detailed applications that a broad selection may be obtained with many resonances whose partial wave functions and decay branch ratios are not clear so far.

From (13), it can be find that the existence of chemical and thermal equilibrium is not definite, even in the infinitive stable system. One finds,

(a) $a_p(p)\tau_{lax} \sim f_T(p)$, $\beta(p)\tau_{lax} \sim 1$: A Steady state. There are no conventional chemical equilibrium and thermal equilibrium.

(b) $a_p(p)\tau_{lax} \gg f_T(p)$, $\beta(p)\tau_{lax} \gg 1$: A special steady state. Only inelastic process is considered, elastic interactions could be neglected.

(c) $a_p(p)\tau_{lax} \ll f_T(p)$, $\beta(p)\tau_{lax} \sim 1$: The system is chemical freeze-out. Only approximate thermal equilibrium is established. Thus, $\mu_i + \mu_{\bar{i}} < 0$.

(d) $a_p(p)\tau_{lax} \ll f_T(p)$, $\beta(p)\tau_{lax} \ll 1$: Both thermal equilibrium and chemical equilibrium are established.

When the boundary conditions is defined,

$$f(0, p, \theta)|_{\cos \theta > 0} = 0 \quad \text{and} \quad 0 \leq f(x, p, \theta) \leq f(\infty, p, \theta), \quad (18)$$

Eq. (12) turns to,

$$f(x, p, \theta) = f_\infty \left[1 - \Theta(\cos \theta) e^{-\frac{\beta(p)\tau_{lax} + 1}{v\tau_{lax} \cos \theta} x} \right], \quad (19)$$

where, $\Theta(x)$ is the step function. From Eq. (19) one finds that although the distribution of particles moving inside varies in positions and directions, the outside particles remain unchanged as f_∞ (shown in Fig. 1).

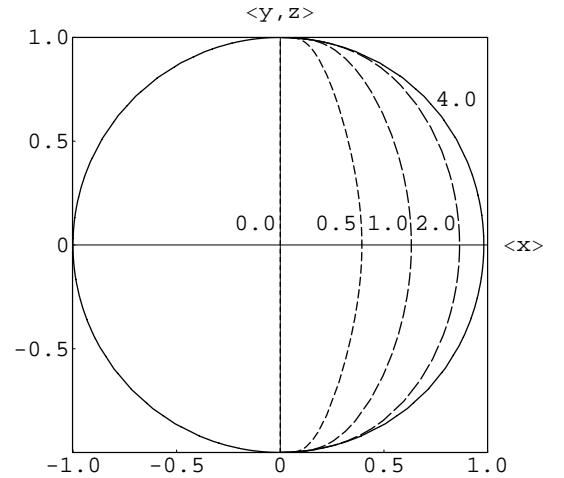


FIG. 1: Transport distribution defined in Eq. (19), normalized by f_∞ . Parameters shown here are values of $\frac{\beta(p)\tau_{lax} + 1}{v\tau_{lax} \cos \theta}$. QGP exists in $x > 0$ region.

For other boundary conditions, such as finite width L of QGP,

$$f_L(x, p, \theta) = f_\infty \left[1 - e^{-\frac{\beta(p)\tau_{lax} + 1}{v\tau_{lax} \cos \theta} [x - \Theta(-\cos \theta)L]} \right], \quad (20)$$

and solitary droplet or glob under homogeneous energy density distribution,

$$f_{IG}(r, p, \theta) = f_\infty \left[1 - e^{-\frac{\beta(p)\tau_{lax} + 1}{v\tau_{lax}} (\sqrt{R^2 - r^2} \sin \theta + r \cos \theta)} \right], \quad (21)$$

solutions could also be deduced, where the rotation of the droplets is neglected (shown in Fig. 2).

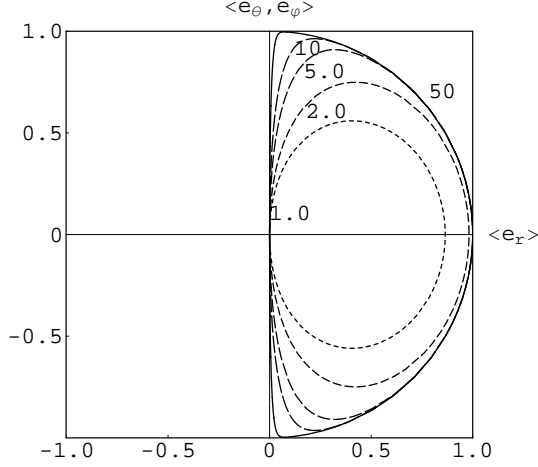


FIG. 2: Transport distribution on the surface for an isolated QGP droplet defined in Eq. (21), normalized by f_∞ . Parameters shown here are values of $\frac{\beta(p)+1/\tau_{lax}}{v} R$.

It can be proved that the influence of the transport is mainly subjected in region near the surface. 98% in $3 L_{in}$, 99.8% in $5 L_{in}$. The emitted hadrons are also created from this region. Considering that the energy density will increase inside the fluid created in the collisions, the hadronization of solidary QGP fluid could be regarded as a kind of surface evaporation. This will access the calculations on the surface despite of the hydrodynamic information inside. But, it is noted that when the fluid breaks into droplets, L_{in} will become much larger. It makes the approximation of evaporation not as good as it was. The density gradient and the time retardation would be involved in the calculations. As a lowest order approximation, these influences are omitted from our calculations on the large amount of hadrons and resonances at the average decouple surface in current stage.

C. Bubbles, Droplets and the Shrinking Surface

When the source is not consist in solidary QGP, but a group of equilibrious bubbles or droplets, the distribution will not change too much. For the infinitive system,

$$f_{EBG}(r, p, \theta) = f_\infty. \quad (22)$$

For the distribution near the bulk surface,

$$f_{EBG}(r, p, \theta) \approx f(x, p, \theta). \quad (23)$$

Even if the hydrodynamics is neglected, the fluid surface will still shrink by the hadron emission. That means the apparent shrinking speed v_s must be considered in the transport equation (9). v_s is not the real particle velocity. When the medium evaporates and the system

expands due to the hydrodynamics, the fluid near the surface will be divided into bubbles and droplets under T_c . η is used to describe the occupation of homogeneous QGP droplets. If the surface could be regarded as a kind of travelling wave approximately,

$$\begin{aligned} f &= f(x - v_s t), \\ \eta &= \eta(x - v_s t), \end{aligned}$$

the Boltzmann Equation turns to

$$-v_s \frac{\partial f}{\partial x} + \frac{p \cos \theta}{E} \frac{\partial f}{\partial x} = \eta \left[\frac{f - f_T}{\tau_{lax}} + a_p - \beta f \right]. \quad (24)$$

The solution is,

$$f(x, p, \theta) = f_\infty \left[1 - \Theta(v \cos \theta - v_s) e^{-\frac{\beta+1/\tau_{lax}}{v \cos \theta - v_s} \int_0^{x(t)} \eta(l - v_s t) dl} \right]. \quad (25)$$

In Eq. (25), the final distribution ($x = -\infty$) will not dramatically change from Eq. (19). Thus, the emission distribution is described as

$$f_{er}(\mathbf{p}) = f_\infty(\mathbf{p})[\mathbf{v} \cdot \sigma_\Sigma - v_s]. \quad (26)$$

where σ_Σ is the outward normal vector of the decouple hyper surface. The idea of Eq. (26) is similar to the Cooper-Frye formulism [37], except for v_s and different hadron distributions. v_s corresponds to the effects of the reabsorption of the freeze-out hadrons by the fluid. It would be helpful to deal with the energy-momentum conservation [38] for the Cooper-Frye formulism. Additionally, the decay corrections are still defined as Eq. (14), (15) and (16).

Thus, the energy loss in the rest frame of the boundary is described as,

$$\begin{aligned} \frac{dE_{emit}}{dt} &= \sum_i \int_{v_i \cos \theta - v_s < 0} -f_{i\infty}(p_i)[v_i \cos \theta - v_s] E_i d^3 \mathbf{p}_i \\ &= \sum_i \left\{ 2\pi v_s \int (1 + \alpha_i) f_{i\infty} E_i p_i^2 dp_i \right. \\ &\quad \left. + \pi \int (1 - \alpha_i^2) f_{i\infty} p_i^3 dp_i \right\}, \end{aligned} \quad (27)$$

where,

$$\alpha_i = \begin{cases} \frac{v_s E_i}{p_i}, & \frac{v_s E_i}{p_i} \leq 1; \\ 1, & \frac{v_s E_i}{p_i} > 1. \end{cases}$$

For momentum loss,

$$\frac{dP}{dt} = \sum_i \int_{v_i \cos \theta - v_s < 0} f_{i\infty}(p_i)[v_i \cos \theta - v_s] p_i \cos \theta d^3 \mathbf{p}_i. \quad (28)$$

If hydrodynamics is neglected, equation

$$\frac{dE_{emit}}{dt} = \varepsilon_b v_s, \quad (29)$$

defines a **minimal shrinking speed** v_{s_0} of the fluid. That implies the bulk evolution does not only depend on hydrodynamics as mentioned in Sec (I). When the average boundary energy density ε_b is small enough to make $v_s = 1$, the local association between different parts of the fluid will completely vanish. So the fluid must be decoupled before

$$\varepsilon_{b_{min}} = \left. \frac{dE_{emit}}{dt} \right|_{v_s=1}. \quad (30)$$

Eq. (30) defines a self-consistent freeze-out limit, which can be used in the hydrodynamic calculations as boundary conditions, together with Eq. (27) and (28).

D. Production Rate

The productions of the color singlets are described in the scenario that two components combine to form a meson or an intermediate baryon state. The baryon productions can be calculated by combining different processes of these $(\frac{1}{2})^\pm$, $(\frac{3}{2})^\pm$ or $(\frac{5}{2})^\pm$ intermediate baryon states [23] (see Appendix A). For simplicity, many-body final channels and direct 3-quark combinations are neglected for their smaller phase space.

The production [35] for each channel is defined as,

$$\frac{d^4 n_{ch}}{d^3 \mathbf{p} dt} = |v_1 - v_2| n_1 n_2 \sigma(p_1 + p_2 \rightarrow p), \quad (31)$$

where,

$$n_i = \int f_i(p_i) d^3 \mathbf{p}_i, \\ \sigma(p_1 + p_2 \rightarrow p) = (2\pi)^4 \int \frac{|M|^2}{4\sqrt{(p_1 \cdot p_2)^2 - m_1^2 m_2^2}} \\ \times \delta^4(p_1 + p_2 - p) \delta(p^2 - m^2) \Theta(E) \frac{d^4 p}{(2\pi)^3}. \quad (32)$$

Thus, the total production rates of baryon states over momentum, where the diquark masses are much larger than those of quarks, can be expressed by [23][19],

$$\frac{dn_{ch}}{dt} = 2\pi^3 |M|^2 \iint f_1(E_1) f_2(E_2) dE_1 dE_2, \quad (33)$$

in the integrating ranges,

$$m_i \leq E_i \leq \infty,$$

and

$$E_1 E_2 \geq \frac{(E_1 + E_2)(m_1^2 E_2 + m_2^2 E_1)}{m^2} + P_{cm}^2,$$

where,

$$P_{cm} = \frac{1}{2m} \sqrt{[m^2 - (m_1 + m_2)^2][m^2 - (m_1 - m_2)^2]}.$$

If the components are under the corrected Ideal Gas Distribution,

$$f_i(p_i) = f_i(E_i) = \frac{\kappa_i}{(2\pi)^3} \frac{\omega_i}{e^{\frac{E_i - \mu_i}{T}} \pm 1},$$

where $\omega_i = 3J_i(J_i + 1)$ is the degeneracy of spin and color, κ_i is the reduction factor caused by the volume effect of bound-state or resonance-state components[34], one has the final particle production rate, (setting the first particle to be fermion,)

$$\begin{aligned} \frac{dn}{dt} &= \sum_{ch} C_{cg}^{ch} \frac{dn_{ch}}{dt} \\ &= \sum_{ch} C_{cg}^{ch} \frac{\omega_1 \omega_2 \kappa |M_{spin}|^2 / 3}{32\pi^3} \\ &\quad \times \iint \frac{dE_1 dE_2}{(e^{\frac{E_1 - \mu_1}{T}} + 1)(e^{\frac{E_2 - \mu_2}{T}} \pm 1)}, \end{aligned} \quad (34)$$

where C_{cg}^{ch} is the weight factor of each channel, and

$$\kappa = [(1 - y_{op}) + C_\alpha y_{op}]^{2-n} (1 - y_{op})^n.$$

Here, n is the number of bound states or resonance states, C_α is the "transparency" of bags, y_{op} is the occupation rate by particle volumes and the factor $1/3$ to $|M_{spin}|^2$ comes from the summation of color indices. The Lorentz-invariant matrix elements $|M_{spin}|^2$ of different effective reactions are listed in Appendix B. For simplicity, we set $C_\alpha = 1$ and get $y_{op} = 0.82 \sim 0.86$ at $T_c \sim 166 \text{ MeV}$.

Supposing that the chemical potentials of the surface would remain still during the evolution, one could find from Eq. (34) that the total relative production ratios of different particles would remain constant no matter how the "fire ball" evolves. This situation is discussed in [23] by setting the same decay cross sections. However, data from the experiments are restricted in specific ranges of transverse momentum and rapidity. They also contain contributions of hard jets. Thus, it is necessary to provide the hadron spectra.

From Eq. (31), one gets

$$\begin{aligned} \frac{d^2 n_{ch}}{4\pi p^2 dp dt} &= \frac{\pi^2 |M|^2}{2 p E} \int dE_2 \frac{(E - E_2) E_2 |\Delta v|}{m P_{cm}} \\ &\quad \times f_1(E - E_2) f_2(E_2), \end{aligned} \quad (35)$$

where,

$$(E - E_2) E_2 |\Delta v| = \sqrt{E E_2 (m^2 - m_1^2 + m_2^2) - (E^2 m_2^2 + E_2^2 m^2)},$$

in the integrating ranges,

$$\begin{aligned} m_2 &\leq E_2 \leq E - m_1, \\ E_2 &\geq \frac{E(m^2 - m_1^2 + m_2^2) - 2mpP_{cm}}{2m^2}, \\ E_2 &\leq \frac{E(m^2 - m_1^2 + m_2^2) + 2mpP_{cm}}{2m^2}. \end{aligned}$$

Correspondingly the expression of $a_{p0}(p)$, which is introduced in Sec (IIB), can be written as,

$$a_{p0}(p) = \sum_{ch} C_{cg}^{ch} \frac{d^2 n_{ch}}{(4\pi p^2) dp dt}. \quad (36)$$

The masses of related particles in "finite temperature" and non-equilibrium system are rather complicated. In this article, current masses of quarks and gluons at zero temperature are used: $m_g = 0$, $m_u = 3MeV$, $m_d = 6MeV$ and $m_s = 95MeV$ [36]. Masses of hadrons and other bound states are expected to increase with temperature or density. This effect is suggested to be relatively small near and below T_c , where the hadronization happens. The increment is about 2% due to a previous calculation [34]. Therefore, hadron mass at zero temperature is used to minimize the large amount of adjustable parameters. Masses diquark and qg state in the deconfinement QGP is not clearly so far. They are estimated from [34], at zero medium effects, which would wipe off the unnecessary influence of the adjustable parameters of that model. The data of diquark are comparable but a bit smaller than some of other estimations from constituent quark models [39]. They are listed below,

$$\begin{aligned} m_{\bar{3}^* 0_{qq}^+} &\approx 485MeV, & m_{\bar{3}^* 1_{qq}^+} &\approx 725MeV, \\ m_{\bar{3}^* 0_{qs}^+} &\approx 580MeV, & m_{\bar{3}^* 1_{qs}^+} &\approx 820MeV, \\ m_{\bar{3}^* 1_{ss}^+} &\approx 905MeV, \\ m_{\bar{3} \frac{1}{2}_{-}^{sg}} &\approx 610MeV, & m_{\bar{3} \frac{1}{2}_{-}^{sg}} &\approx 715MeV. \end{aligned}$$

III. HYDRODYNAMICS

The ideal fluid satisfies the local conservation of energy and momentum,

$$\frac{\partial T_{\mu\nu}}{\partial x_\mu} = 0, \quad (37)$$

and the local charge conservation

$$\frac{\partial j_\mu^i}{\partial x_\mu} = 0, \quad (38)$$

where j^i refers to the baryon current, strange current, etc.

The Equation of State (EOS) for SQGP [34] is complicated. Concerning there are no thermalized mix phases in current scenario, the EOS will become differentiable compared with the EOSQ [6][18] from bag models. As a preliminary attempt to apply the hydrodynamic calculation with evaporation boundary conditions, the EOS is simply set to be $\varepsilon = 3P$ if no thermalized hadronic phase is involved.

Bag constant B is not a parameter in our calculations. In SQGP, the contribution of bound states such as diquarks, which are already counted in the statistical properties, is equivalent to the bag constant. The separated

droplets also contribute ε and P under similar styles. On the other hand, concerning that only one phase is considered and the form in Eq. (37) can be written in $\varepsilon + P$ and $\partial \ln P$, the transform

$$\varepsilon' = \varepsilon + B, \quad P' = P - B,$$

shows no difference, except on the boundaries.

A. Boundary Conditions

When the hadronization is coupled to the hydrodynamics by the boundary conditions, Eq. (37) is expressed by

$$\frac{\partial T_{\mu\nu}}{\partial x_\mu} = \frac{dT_{0\nu}}{dt}. \quad (39)$$

It will be associated with the solutions of the Transport Equation (9). For simplification, the hadronization loss is only defined in the decoupling hyper surface, which is shrinking at the apparent speed v_s . Thus, the boundary condition could be deduced from Eq. (27), (28) and (30) in the FCT hydrodynamic calculations [40][30]. The evolution of the decoupling hyper surface is both determined by the evaporation and hydrodynamic expansion.

B. Spherical Expansion

Spherical expansion is discussed to demonstrate the influence of boundary conditions. When the EOS is simplified, the 1 + 1 Hydrodynamics could be handled in a simple way [41],

$$\begin{aligned} \frac{\partial \xi}{\partial t} &= -\frac{2}{3-v^2} \cdot \left[v \frac{\partial \xi}{\partial r} + 2 \frac{\partial v}{\partial r} + 2(N-1) \frac{v}{r} \right], \\ \frac{\partial v}{\partial t} &= -\frac{1}{3-v^2} \cdot \left[\frac{3(1-v^2)^2}{4} \frac{\partial \xi}{\partial r} + 2v \frac{\partial v}{\partial r} \right. \\ &\quad \left. - (N-1) \frac{v^2(1-v^2)}{r} \right], \end{aligned} \quad (40)$$

where N corresponds the system dimension, and

$$\xi = \ln \frac{\varepsilon + P}{\varepsilon_b + P_b} = C \ln(\varepsilon + P) = C' \ln \varepsilon.$$

For spherical expansion $N = 3$.

The evolutions under different evaporation boundary conditions are shown in Fig. 3 - Fig. 5. The system is set to be $R_0 = 4.44 fm$ under a Gaussian distribution with $\varepsilon_{center} = 9 \varepsilon_b$. The initial expansion is set to be $u(r)/r = 0.05 fm^{-1}$. The minimal shrinking speed is set to be 0.05, 0.50 and 0.85 separately. It is shown in the calculations that the evaporation plays an important role when the system expansion is small. When the expansion is large, the evolution is dominated by the hydrodynamics.

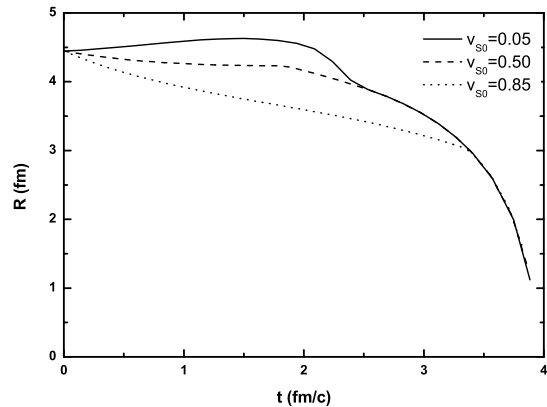


FIG. 3: Hydrodynamic evolutions of the decoupling hyper surface in spherical expansions under different minimal shrinking speed v_{s0} .

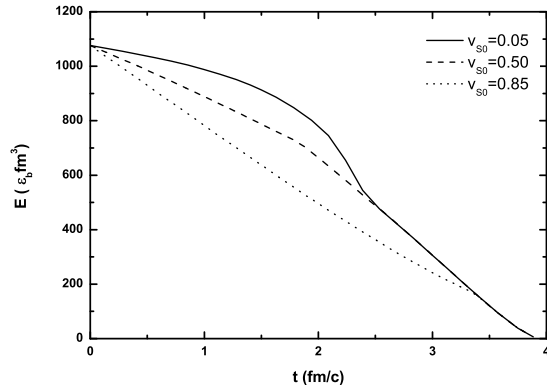


FIG. 4: Hydrodynamic evolutions of the bulk energy in spherical expansions under different minimal shrinking speed v_{s0} .

C. Cylindrical Expansion

The evolution in central event in RHIC is more similar to a kind of cylindrical expansion. A $2+1$ evolution was tried under evaporation boundary conditions. Unfortunately, the calculation failed in stability by the interpolations and extrapolations on the curved boundary. This problem is not resolved completely so far. Thus, the transverse evolution with longitudinal invariant boost is applied in our calculations.

The initial conditions is estimated from the Glauber Model [42]. Parameters are selected to be the same values in [6][18] for RHIC Au-Au 200 GeV. The formation time of the thermalization is set to be $\tau_0 = 0.6$ fm/c. The real expansion may be more rapid than the Bjorken boost in a longitudinal calculation from Eq. (41). It is shown in the calculations that the contributions to the the evolution caused by the evaporation boundary condi-

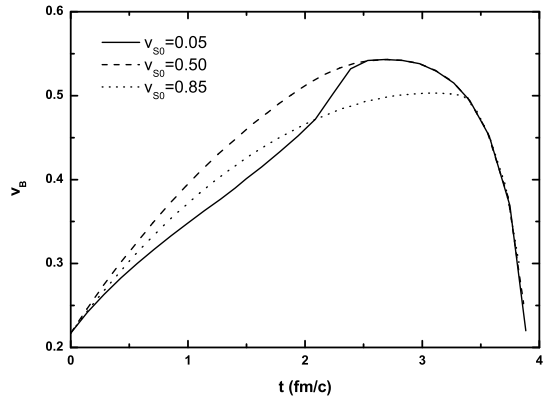


FIG. 5: Hydrodynamic evolutions of the velocity on the boundary in spherical expansions under different minimal shrinking speed v_{s0} .

tions are small, except in the very beginning period. This is due to the large longitudinal expansion, which makes it possible to apply a conventional hydrodynamics with a cut in the decoupling hyper surface when hadronization is calculated. The simulation of elliptic flow in this model may be also accessible in future calculations.

The results of the evolution are shown in Fig. 6 and Fig. 7. The system evolves in $8 - 9$ fm/c with a monotonic decrease of the radius. It is noted that the initial transverse expansion will make remarkable consequences. However, it is set to be zero to compare with the existing calculations [6][18]. The calculations also showed that the chemical potential remained still approximately during the evolution. It is due to the large longitudinal boost too.

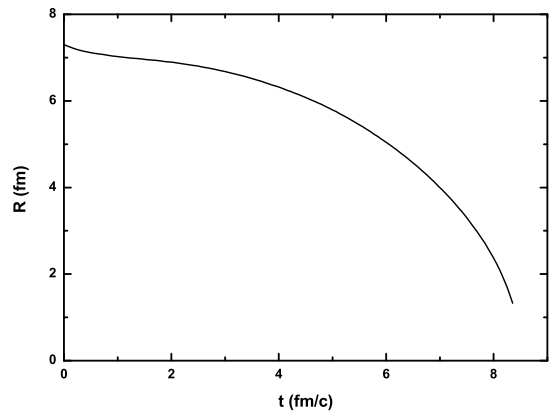


FIG. 6: Hydrodynamic evolution of the mean decoupling hyper surface in RHIC 200 GeV central events.

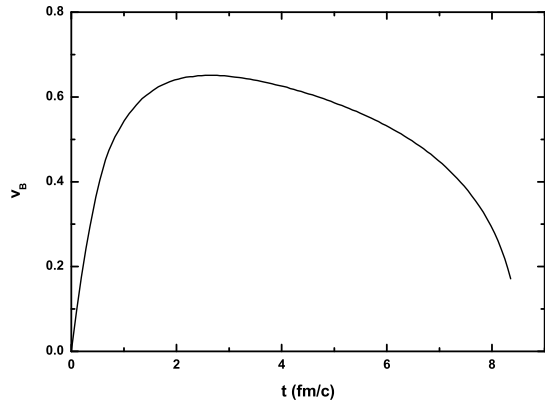


FIG. 7: Hydrodynamic evolution of the velocity on the boundary in RHIC 200 GeV central events.

D. Reabsorption and decay

The slow hadrons emitted in early stage may be reabsorbed or pushed by the expanding source. Fortunately, the system shrinks. The decay products can also be absorbed. The influence can be calculated by tracing each particles. While, the feedback to the system is too complicated to apply. Considering the shrinking speed v_s in the local rest frame is near 1 at the beginning of the evolution and exceeds 1 in the later stage. The corrections are expected to be small. Vertex cuts in the measurements are also omitted, although it is possible to apply them. Accordingly, decay contributions from K^\pm and K_L^0 are neglected from π productions.

IV. APPLICATIONS

A. Hadron Spectra in Central Events

As the first application of our model, soft hadron production spectra in RHIC $Au - Au \sqrt{s_{NN}} = 200 \text{ GeV}$ in central events are calculated, compared with experimental data [43, 44, 45, 46, 47, 48, 49, 50, 51, 52, 53, 54, 55]. When the effective evaporations are applied, the flat surface transport result Eq. (19) is used instead of a complicated expression of curved surface, eg. Eq. (21).

The critical temperature for QGP phase transition is set to be $T_c = 166 \text{ MeV}$ in RHIC $Au - Au 200 \text{ GeV}$ conditions. The $T_c \sim \mu_B, \mu_S$ relations [56][57] are not inserted in detail. The average meson-parton inelastic cross section $\langle \sigma_m \rangle$ is set to be 7 mb . As SQGP is discussed, the critical energy density is set to be $\varepsilon_c \approx 1.236 \varepsilon_{SB} = 1.909 \text{ GeV}/\text{fm}^3$ due to the boundary states or resonance states compensations [34], which are equivalent to the effect of the bag parameter. The volume occupation rate for none-point components in SQGP is

set to be $y_{op} = 0.827$ due to the same calculation. The results are not sensitive to y_{op} , because the adjustable g_B^2 includes the influence of the uncertainty of y_{op} partially. The influences of the elastic interaction τ_{lax} , which corresponds a thermalization process, are different for different hadrons and in different momentum regions, by a systematic comparison with final hadron spectra. The thermalization for π or K is large, but for Ω is small. To minimize the free parameters, especially hadron specific parameters in this stage, τ_{lax} is set to be ∞ for all hadrons. All data listed in this subsection is none-thermalization data, although partons are supposed to be thermalized. Discussions of the influence of elastic interaction and hadron rescattering are presented in Sec (IV A 6).

Proton and π spectra in PHENIX [43] are used to fit the parameters of $\langle \eta \rangle$, μ_B , g_B^2 and g_M^2 . Phase equilibriums Eqs. (1) are applied in RHIC conditions to estimate g_M^2 and ε_b . When μ_B and T_c are fixed, the charge conservation could be removed. By comparing an averaged energy and momentum conservation through Eqs. (1), (27) and (28), one could get $\varepsilon_{b_{min}} = 0.085 \varepsilon_c$. It is a lower limit. Through the slopes presented in [43], the decoupling SQGP droplet occupation is set to be $\langle \eta \rangle = 0.11$. It is noted that the hadrons moving between SQGP droplets are not counted in the fluid.

Thus, the parameters are extracted or estimated,

$$\begin{aligned} g_M^2 &= 0.73 \frac{\langle \sigma_m \rangle}{mb} = 5.11, \\ g_B^2 &= 6.7 g_M^2 = 34.24, \\ \mu_B &= 27 \text{ MeV}, \\ \varepsilon_b &= \langle \eta \rangle \varepsilon_c, \\ \langle \eta^{-1} \rangle &\approx \frac{1}{\langle \eta \rangle}. \end{aligned}$$

The minimal shrinking speed is determined by Eq. (29), $v_{s_0} = 0.222$. The evolution duration for the fluid is about $8.4 \text{ fm}/c$. The strange chemical potential is determined by the strange conservation,

$$\mu_S = \frac{\mu_B}{3} - \mu_s = 9.35.$$

There is no independent parameters for the strange particles other than the masses of quarks and diquarks, which are not adjustable in the calculations. The possible suppression for strange partons are not introduced in present stage.

1. Invariant Productions

The hadron invariant production can be calculated through the method below,

$$\begin{aligned} \left. \frac{d^2 N_i}{2\pi p_T dp_T dy} \right|_y &= \frac{d}{2\pi p_T dp_T} \sum_j \int f_{er_j}(\mathbf{p}_j'') dS dt' d^3 \mathbf{p}_j' \\ &\quad F_{D_{ji}}(\mathbf{p}_j', \mathbf{p}_i') \delta(y_L + y_i' - y) \\ &= \frac{d}{2\pi p_T dp_T} \sum_j \int \{ d\theta dt'' d^3 \mathbf{p}_j'' dy_L \delta(y_L + y_i' - y) \\ &\quad Rt' \gamma_L^{-1} \left(\frac{du_L}{dy_L} \right) f_{er_j}(\mathbf{p}_j'') F_{D_{ji}}(\mathbf{p}_j'', \mathbf{p}_i') \}. \end{aligned} \quad (41)$$

Where $dt'' = \gamma_b(dt' - v_b dR)$ is the evolution step with transverse fluid velocity v_b on the hadronization surface and $(du_L/dy_L) = \gamma_L$. The superscript (") is related to the local rest frame of the hadronization surface, (') is related to the evolution in the rest frame of rapidity y_L according to laboratory frame, f_{er} is the emission rate and F_D is the decay contribution with corrections of re-absorption and vertex cut off. If the transport term of decay products is combined, a factor $\alpha_{i,j}$ defined in Eq. (16) will be applied to F_D (Sec II B).

Integration of Eq. (41) is obtained by Monte-Carlo simulations, which partially trace the directly emitted hadrons. By counting enough events, the statistical errors for dN/dy caused by random simulations are less than 0.5% – 1% for different hadrons. The statistical errors for p_T distributions are relatively larger. They are particularly large in very low p_T and high p_T regions. The reason in low p_T is due to the sensitivity of denominator p_T in Eq. (41). The later one is due to the low hadron abundance in high p_T area. In the region of 0.3 – 4 GeV, the statistical errors are expected to be smaller than 5% for most spectra.

It should be noted that the compensation of in-transport decay contribution $\alpha_{i,j}$ would cause an algorithmic problem, when feed down corrections are applied, although it simplifies the calculations. In our algorithm, the in-transport decay contributions will be removed from the spectra together with the final decay contributions. But this amount of hadrons can not be reconstructed in the experiments, because their decay products may be changed in species or momentum in the transport process. Thus, the feed down corrections are expected to be larger than those in experimental analysis, and the exclusive spectra are expected to be smaller. As most of feed down corrections are applied for weak decays, whose life times are large enough, this algorithmic problem is expected small.

2. Particle Selections

The light hadron productions are dominated by decay products. For example, the amount of direct pion is less

than 5% of all pion abundance. Considering the convergence of heavy resonance decay contribution is slow, many resonances need to be added in our calculations. As discussed in Sec (II B) Eq. (16), the width of the resonances will not decrease the contributions to their decay products. Thus, the selection is subjected to their relative production rates and branch ratios compared with their daughter particles, which are counted in our results. For example, when baryon octet and decuplet are discussed in the results, more heavier resonances should be added. N baryons are counted up to $N(1535)$ for their contributions to proton, while Λ baryons are counted up to $\Lambda(1830)$ (leaving $\Lambda(1800)$) for their contributions to $\Sigma^*(1385)$. Only hadrons greater than (**) [36] are considered.

0^-	1^-	0^+	1^+	2^+
π	ρ	a_0 980	b_1 1235	K_2 1430
K	K_{892}^*	f_0 600	h_1 1170	
η	ω	f_0 980	a_1 1260	
η'	ϕ	K_0 1430	f_1 1285	
	K_{1410}^*		K_1 1270	
			K_1 1400	

TABLE I: Mesons selected in the calculations.

N	Δ	Λ	Σ	Ξ	Ω
N_{938}	Δ_{1232}	Λ_{1116}	Σ_{1192}	Ξ_{1317}	Ω_{1672}
N_{1440}	Δ_{1600}	Λ_{1405}	Σ_{1660}	Ξ_{1530}	
N_{1520}	Δ_{1620}	Λ_{1520}	Σ_{1670}	Ξ_{1690}	
N_{1535}		Λ_{1600}	Σ_{1750}	Ξ_{1820}	
		Λ_{1670}	Σ_{1775}		
		Λ_{1690}			
		Λ_{1830}			

TABLE II: Baryons selected in the calculations.

Mesons and baryons calculated in our model are listed in Table I and II. Although some of 0^+ particles, such as $f_0(600)$, $f_0(980)$ and $a_0(980)$ are often interpreted as non- $q\bar{q}$ states, they are still treated as scalar mesons in the calculations.

It is impossible to take all resonances with precise properties into accounts. Thus, the effective coupling constants g_M and g_B are already containing the normalization factors. The more resonances are considered, the smaller coupling constants are obtained. The effect of the normalization depends on the hadron selection, which may provoke systematic errors into final results. For example, many of the non-strange heavy mesons will decay to three pions, strange heavy mesons will decay to two pions and one kaon. Considering there are four final kaons and only three pions, the K/π ratio would drop when more $8 + 1$ heavy mesons are inserted.

Another example is about ϕ and Ω . Almost none of the hadrons could decay to them. An incomplete hadron list

will provoke a promotion to them relative to the other hadrons. Unfortunately, many heavy resonances are in lack of some essential properties such as spin and branch ratios, or even the probabilities of their existences.

3. Spectra

Hadron spectra and relative ratios are shown in Fig. 8 - Fig. 29. The corresponding experimental data are corrected by various treatments, which will be explained in the captions of those figures. As exclusive protons and inclusive pions in PHENIX [43] are used to fit parameters, the satisfaction for these data are better than the others, as presented in Fig. 8, Fig. 9 and Fig. 10.

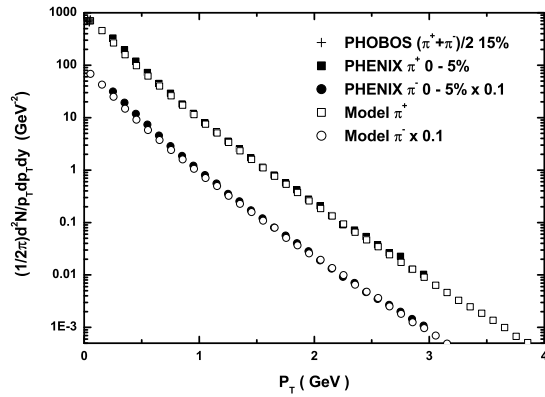


FIG. 8: Invariant productions of π^\pm compared with PHENIX [43] and PHOBOS [44] data at 200 GeV . The abundances are inclusive, no feed down corrections are applied. Relaxation time $\tau_{lax} \rightarrow \infty$ for all figures.

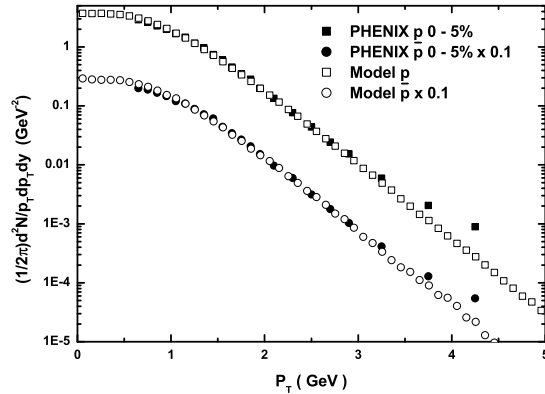


FIG. 9: Invariant productions of (anti-)proton compared with PHENIX data [43] at 200 GeV . Feed down corrections from Λ are applied.

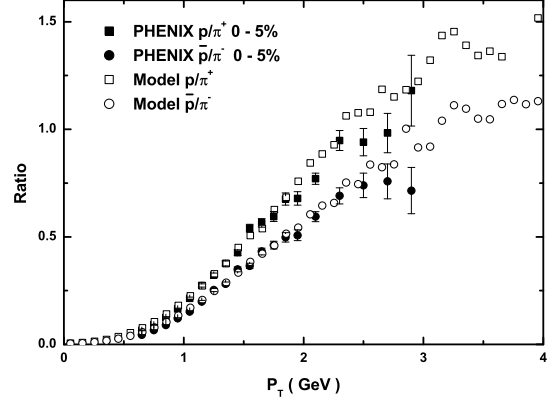


FIG. 10: p/π^+ and \bar{p}/π^- ratios compared with PHENIX data [43] at 200 GeV . Feed down corrections are the same as in Fig. 8 and Fig. 9.

As only soft productions, where hadrons are recombined from thermal partons, are taken into accounts, high p_T spectra can not be reproduced correctly in our model. It is presented clearly in Fig. 11 and Fig. 12 compared with STAR high p_T data [45], where proton spectra are inclusive, pions are corrected from Λ and K_S^0 decay contributions. The effects of jets or shower partons in high p_T range are more significant for pions and protons than the other heavy resonances, especially multi-strange heavy resonances.

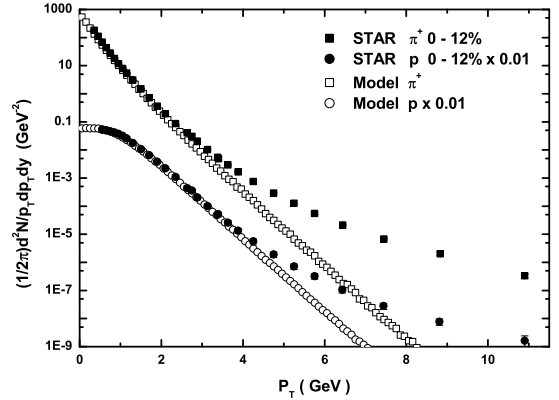


FIG. 11: Invariant productions of proton and π^+ compared with STAR data [45] at 200 GeV . Spectrum for proton is inclusive. Decay contributions from Λ and K_S^0 to pions are removed.

Charged kaon distributions are shown in Fig. 13. The model gives larger distributions than the experimental data. Various reasons may cause this phenomenon. Lack of heavy resonances outside our hadron list, may be one of them. Another issue is about the strange quark mass.

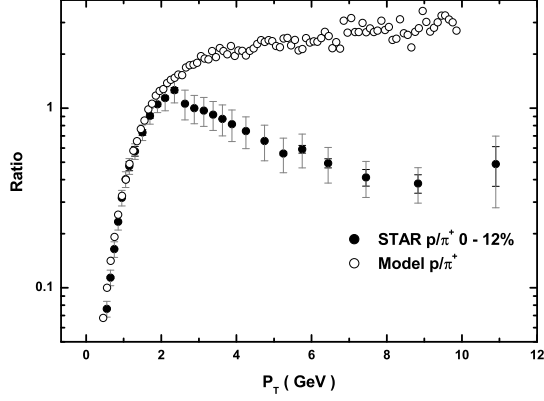


FIG. 12: p/π^+ ratios compared with STAR data [45] at 200 GeV . Spectrum for proton is inclusive. Decay contributions from Λ and K_S^0 to pions are removed.

$m_s = 95 MeV$ [36] is used here. Heavier strange quark mass, such as $m_s = 170 MeV$ can reduce kaons by 5%. It will also reduce the multi-strange baryons ($\Sigma^*(1385)$, $\Xi^*(1530)$ and Ω), which are already smaller than expected, unless the strange diquark abundances are enhanced. Thermalization and inelastic rescattering are other hopeful candidates. When the relaxation time is set to be $\tau_{lax} \sim 1 fm/c$, the kaon spectrum can be well reproduced. The multi-strange baryons will decrease too, because they can be hardly thermalized. Detailed discussion on thermalization and rescattering will be presented in Sec (IV A 6).

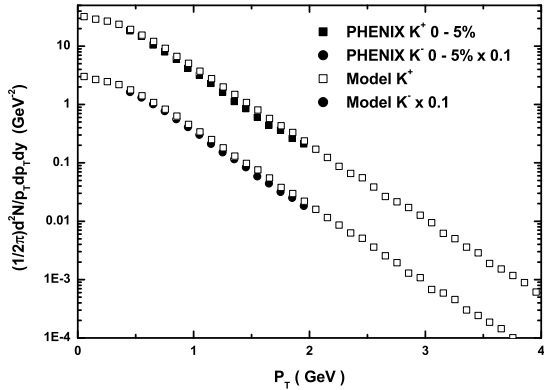


FIG. 13: Invariant productions of K^\pm compared with PHENIX data [43] at 200 GeV . The abundances are inclusive, no feed down corrections are applied.

Λ and Ξ^- spectra are shown in Fig. 14 and Fig. 15. The data for Ξ are well satisfied. The results for Λ and $\bar{\Lambda}$ are smaller in low p_T regions, especially for positive Λ . A general character of the model results is the enhancement of strange mesons and reduction of

strange baryons. That implies the disadvantages of some simplified assumptions. Hadron rescattering, such as $N + \bar{K} \rightleftharpoons \Sigma(\Lambda) + \pi$ or $N + \bar{K} \rightarrow \Sigma^*(\Lambda^*) + X$, may be a possible reason. Another favorite reason is about the properties of diquarks. Diquarks are supposed under ideal Bose distributions in SQGP. But the transport distribution Eq. (13) may be suitable for them due to their heavy masses. The promotion from thermal distributions are promotional to their masses in low momentum regions, as in the issues of hadrons. If the production of diquarks is applied with proper mass and width, the low p_T data may be described better. From this view, the baryon coupling constant g_B is combined with a diquark coupling constant g_D inside.

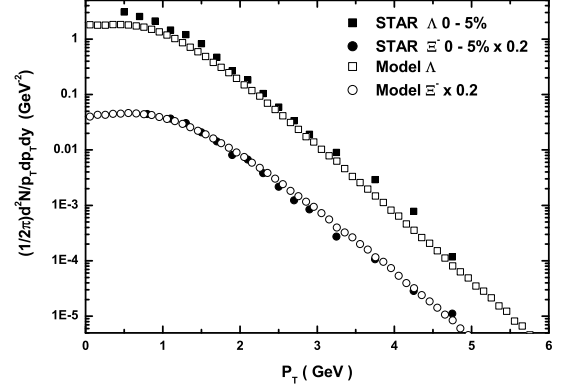


FIG. 14: Invariant productions of Λ and Ξ^- compared with STAR data [46][47] at 200 GeV . The data of Ξ^- is inclusive. Decay contributions from Ξ^- , Ξ^0 and Ω to Λ are removed. Decay contributions from Σ^0 are included.

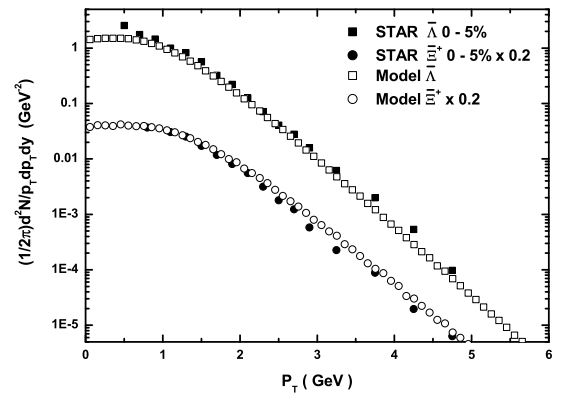


FIG. 15: Invariant productions of $\bar{\Lambda}$ and Ξ^+ compared with STAR data [46][47] at 200 GeV . Decay treatments are the same as in Fig. 14.

Comparison of Λ and K_S^0 are shown in Fig. 16 and Fig. 17. The enhancement of K and reduction of Λ are

displayed more clearly in the comparison. It is noted that the inclusive Λ distribution, for which no feed down corrections were done, seems much better than those in Fig. 14 compared with corresponding STAR data. Different to the soft p/π ratios, soft Λ/K ratios start to drop after 4 GeV .

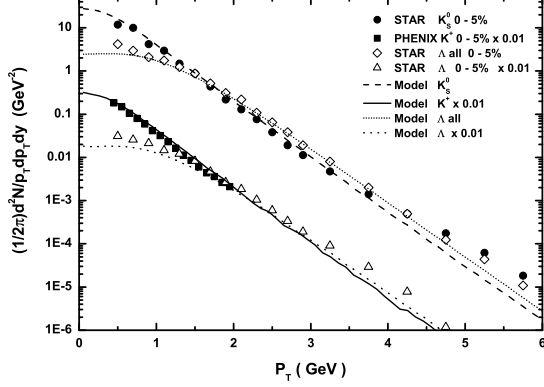


FIG. 16: Invariant productions of Λ , K^+ and K_S^0 compared with STAR data [46][47][48] at 200 GeV . Data for K_S^0 and Λ "all" are inclusive. Other decay treatments are the same as in Fig. 14.

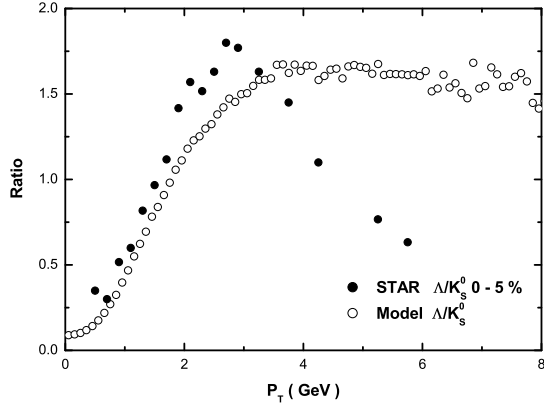


FIG. 17: Λ/K_S^0 ratios compared with STAR data [48] at 200 GeV . The abundances are inclusive, no feed down corrections are applied.

$K^*(892)$ production is shown in Fig. 18. The in-transport decay (ITD) loss Eq. (15) plays an important role in the final spectrum. Considering that the meson inelastic cross section is supposed to be $\frac{2}{3}$ of baryon cross section, the in-transport decay losses of mesons would be more significant than those of baryons with similar widths. $\langle\eta^{-1}\rangle \approx \langle\eta\rangle^{-1}$ is locked in the calculations. ρ^0 and ω suppressed distributions are shown in Fig. 19, as predictions for $Au-Au$ 200 GeV central events.

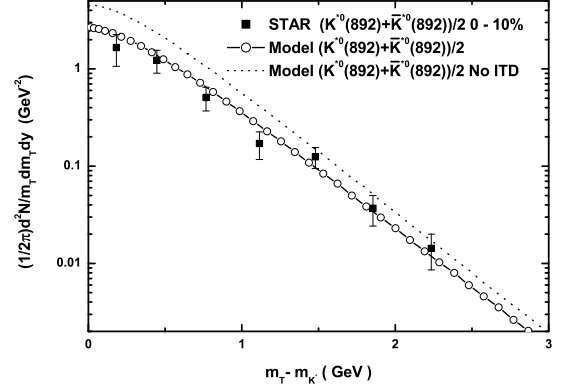


FIG. 18: Invariant production of $(K^*(892) + \bar{K}^*(892))/2$ compared with STAR data [49] at 200 GeV . The data are inclusive. Dotted line shows the situation without in-transport decay (ITD) loss corrections.

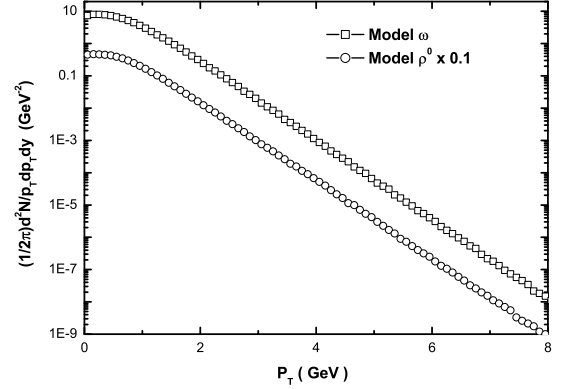


FIG. 19: Expected invariant productions of ρ^0 and ω at 200 GeV . The data are inclusive.

ϕ production is shown in Fig. 20. The model results are larger than the measurements, partially because of the limited hadron list as discussed. Heavier strange quark mass can not reduce it much. Upgrading the model to deduce the elliptical flow of ϕ [58] or to simulate the full transports in future stage may be helpful to determine the reason. As shown in Fig. 20, the STAR data [50] are about two times of the PHENIX data [51]. Further measurements may be required to draw a conclusion.

$\Sigma^*(1385)$ distributions are shown in Fig. 21. Theoretical results are smaller than the experiments, especially in very low p_T region. The situation is similar to Λ . $\Lambda\pi$ or $N\bar{K}$ process may regenerate some of $\Sigma^*(1385)$ [52][53]. As $\Sigma^*(1385)$ can not decay to $N\bar{K}$ for its low mass, it may become a one-way valve to deliver strange quarks from K to $\Lambda(\Sigma)$. Because many heavy resonances which would decay to $\Sigma^*(1385)$ are in lack of their detailed properties and only a part of them may be inserted to the baryon list

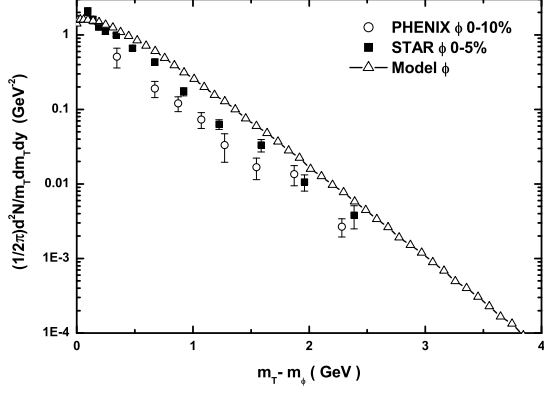


FIG. 20: Invariant production of $\phi(1020)$ compared with STAR [50] and PHENIX [51] data at 200 GeV . The data are inclusive.

(see Table II), the production could probably be reduced by such way too.

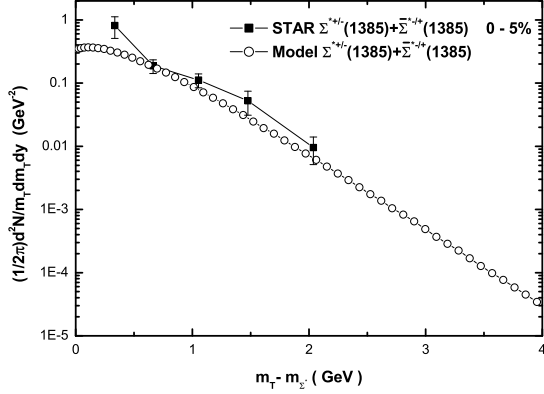


FIG. 21: Invariant production of $\Sigma^{*\pm}(1385) + \bar{\Sigma}^{*\mp}(1385)$ compared with STAR data [52] at 200 GeV . The data are inclusive.

Invariant productions of $\Xi^{*0}(1530)$ and Ω are shown in Fig. 22. The calculated distribution of Ω is small in low p_T and a little large in high p_T . It looks the Ω has different slope parameters, if it is treated in thermal decouple models. The fact, the spectrum is not as large as ϕ shows that either enough baryons were considered compared with total baryon productions, or some of the heavy resonances were over estimated. The spectrum of $\Xi^{*0}(1530)$ is bad. It might be due to the fact, that $\Xi(1950)$ is not counted in our model. $\Xi(1950)$ is a mysterious baryon. Neither spin, parity nor branch ratios are clear. It is even suggested that there might be more than one Ξ existed in that mass [36].

Ω over ϕ ratios are presented in Fig. 23. As multi-strange hadrons, the jet contributions for ϕ and Ω are

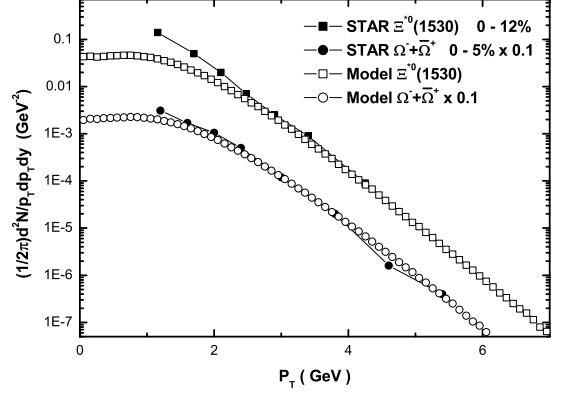


FIG. 22: Invariant productions of $\Xi^0(1530)$ and $\Omega + \bar{\Omega}$ compared with STAR data [53][46][47] at 200 GeV . All data are inclusive.

expected to be small, as one can find it in their spectra in Fig. 20 and Fig. 22. Thus the results are similar to the results of recombination [12]. The decrease in the experiments may be due to fluctuations.

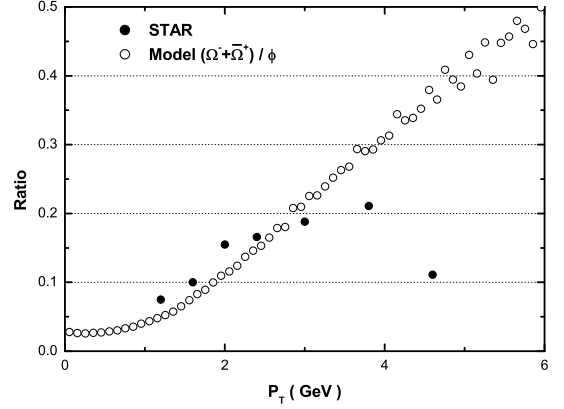


FIG. 23: Ratios of $(\Omega^- + \bar{\Omega}^+)/\phi$ compared with STAR data [55]. All data are inclusive.

From the data discussed above, there seems to be two slopes exist in some of the hadron spectra. A boost in low p_T regions is significant. A possible reason is that, the theoretical values at low p_T may be suppressed by the surface evaporation, which are not suitable in the later stage of the evolution. But it is not easy to tell if the phenomena are due to statistical errors or due to some physical principles.

Some of the total ratios are listed in Table III. The comparing data are from [43] and [54]. It is noted that the data from [54] correspond to baryons in p_T range of 2.4 – 3.6 GeV and mesons in p_T range of 1.6 – 2.4 GeV . The influences of decay are relatively small in those

ranges. The strange baryon ratios extracted from [54], are similar to the data in 130 GeV [59][60][61]. Some of the corresponding data are shown in Fig. 24 and Fig. 25.

dN/dy data are not listed to compare with the experiments. It is because many of the dN/dy data are extracted from Boltzmann fits, which would always increase when p_T drops. However, some of our spectra for baryons will decrease when p_T drops. Thus, our estimations are always smaller, no matter how well they could fit the measurements.

Particles	Model	Exp
π^-/π^+ (in)	1.006	$0.984 \pm 0.004 \pm 0.057$ [43]
π^-/π^+ (ex)	0.999	1.01 ± 0.02 [54]
K^-/K^+	0.915	$0.933 \pm 0.007 \pm 0.054$ [43]
		0.96 ± 0.03 [54]
\bar{p}/p (ex)	0.748	$0.731 \pm 0.011 \pm 0.062$ [43]
\bar{p}/p (in)	0.783	$0.747 \pm 0.007 \pm 0.046$ [43]
		0.77 ± 0.05 [54]
$\bar{\Lambda}/\Lambda$	0.844	0.72 ± 0.024 [54]
Ξ^+/Ξ^-	0.907	0.82 ± 0.05 [54]
$\bar{\Omega}^+/\Omega^-$	1.011	1.01 ± 0.08 [54]
K^+/π^+	0.203	$0.171 \pm 0.001 \pm 0.010$ [43]
K^-/π^-	0.184	$0.162 \pm 0.001 \pm 0.010$ [43]
p_{ex}/π^+	0.0645	$0.064 \pm 0.001 \pm 0.003$ [43]
p/π^+ (in)	0.102	$0.099 \pm 0.001 \pm 0.006$ [43]
\bar{p}_{ex}/π^-	0.0479	$0.047 \pm 0.001 \pm 0.002$ [43]
\bar{p}/π^- (in)	0.0797	$0.075 \pm 0.001 \pm 0.004$ [43]

TABLE III: Some relative hadron ratios compared with RHIC data [43][54] at 200 GeV . Data from [54] correspond to baryons in p_T range of 2.4 – 3.6 GeV and mesons in p_T range of 1.6 – 2.4 GeV . The statistical errors in the model are up to 5%.

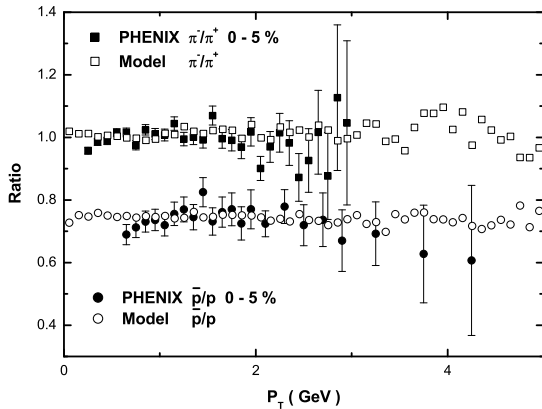


FIG. 24: Inclusive π^-/π^+ and exclusive \bar{p}/p ratios compared with PHENIX data [43] at 200 GeV .

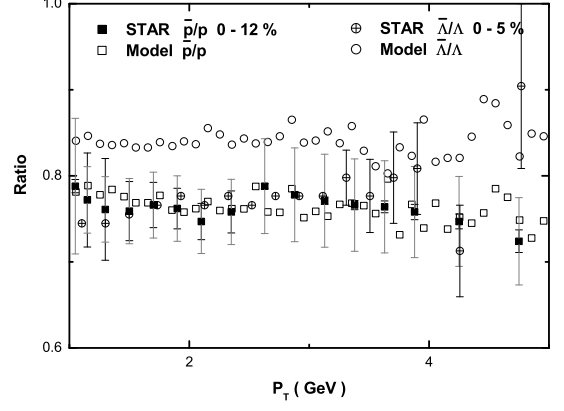


FIG. 25: Inclusive \bar{p}/p and inclusive $\bar{\Lambda}/\Lambda$ ratios compared with STAR data [45][48] at 200 GeV .

4. Σ^0 and Λ

Σ^0 and Λ data are good samples to discuss the hadronization models. Some string fragmentation models require $\Sigma^0/\Lambda \sim 0.35$. Thermal statistical models predict 0.65 – 0.75 due to the mass difference. If the hadronization is dominated by gluon junction or coalescence, the ratio is about 1. In our case, which is similar to the coalescence or recombination, the result is a little larger than 1 for direct recombined Σ^0 and Λ emitted from SQGP [23][19]. This is because the Σ^0 contains the largest term $B_{\frac{1}{2}}(A_{ud}, s)$, as described in Eqs. (A2), Appendix A. This term does not exist in the isospin-0 Λ .

With parameters selected above, the direct ratio $\Sigma^0/\Lambda \sim 1.181$. Considering the decay contributions from heavy baryons or resonances, the ratio will decrease to 0.636 instead. Plots of direct Σ^0 and Λ spectra, inclusive Σ^0 spectrum and exclusive Λ spectrum with Σ^0 decay contribution removed, are shown in Fig. 26. The corresponding ratios in different p_T ranges are shown in Fig. 27.

Considering the difficulties to extract Σ^0 by the electromagnetic decay, Σ^\pm productions may be easier to reconstruct if π^0 is well measured in EMC. Their productions are supposed to be similar to Σ^0 . The expected Σ^+ productions are shown in Fig. 28.

$\Lambda(1405) 0(\frac{1}{2}^-)$ and $\Lambda(1520) 0(\frac{3}{2}^-)$ are regarded as singlet states. It is not easy to determine their wave functions in quark-diquark model. More over, whether $(L = 1, S = \frac{3}{2})$ or $(L = 1, S = \frac{1}{2})$ can not be distinguished. Coarse estimations on $\Lambda(1405)$ and $\Lambda(1520)$ at 200 GeV are shown in Fig. 29 based on specific wave function assumptions. Here $\Lambda(1405)$ is supposed to be $(L = 1, S = \frac{1}{2})$, octet instead. $\Lambda(1520)$ is supposed to be $(L = 1, S = \frac{3}{2})$, octet as Eq. (A3) in Appendix A.

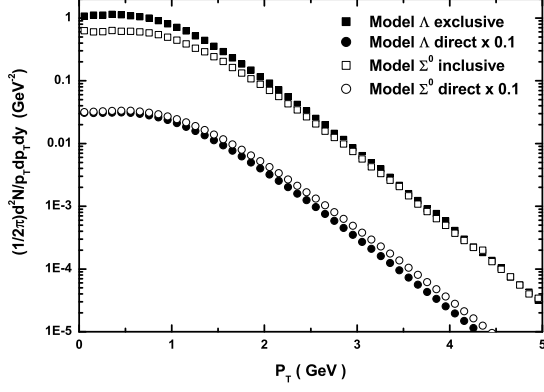


FIG. 26: Expected invariant productions of direct Σ^0 , direct Λ , inclusive Σ^0 and exclusive Λ at 200 GeV . Decay contributions from Σ^0 , Ξ^- , Ξ^0 and Ω to the exclusive Λ are removed.

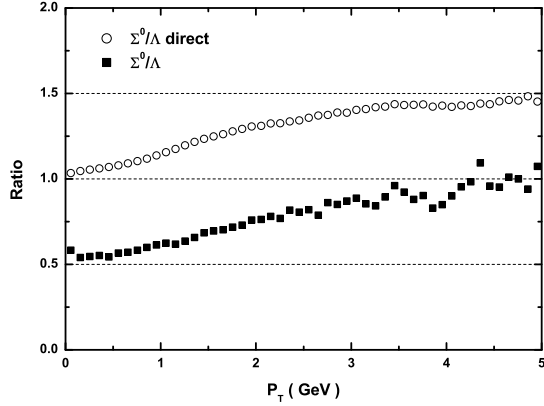


FIG. 27: Related Ratios for Fig. 26. Decay treatments are the same.

5. $\bar{\Omega}^+/\Omega^-$ Ratio

When diquarks are inserted to the Quark Gluon Plasma, the strange chemical potential of the system will increase due to the negative strange numbers of us and ds diquarks. In the calculations, the strange chemical potential is extracted from the strange conservation,

$$\mu_S = \frac{\mu_B}{3} - \mu_s = 9.35.$$

Thus the strange quark and ss diquark will contain negative chemical potentials, $\mu_s = -0.35$, $\mu_{ss} = -0.7$. This situation was well discussed in [19]. Other discussions from string fragmentation [62] with diquarks gave similar conclusions. Calculations without diquarks will give $\bar{\Omega}^+/\Omega^- \leq 1$ [63][3].

As shown in Table III, the ratio of $\bar{\Omega}^+/\Omega^- = 1.011$ is consistent with the STAR measurements [54]. Con-

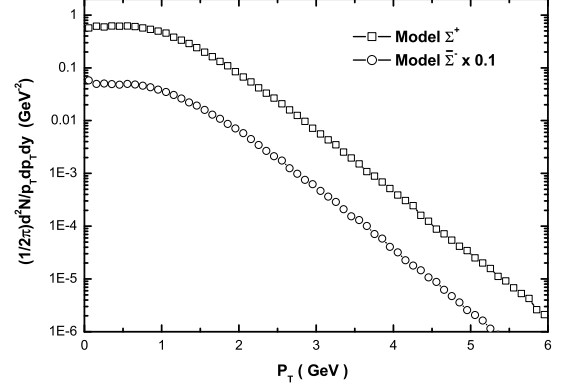


FIG. 28: Expected invariant productions of direct Σ^+ and Σ^- at 200 GeV . No feed down corrections are applied.

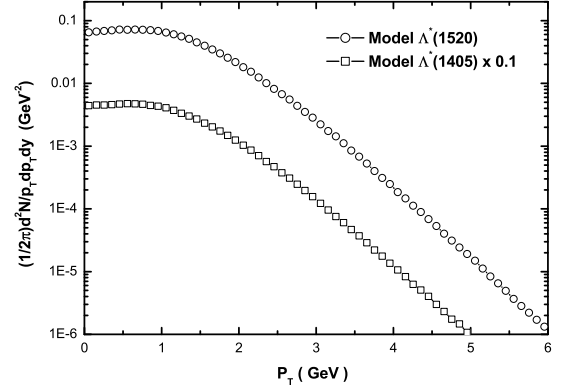


FIG. 29: Expected invariant productions of direct $\Lambda(1405)$ and $\Lambda(1520)$ at 200 GeV . No feed down corrections are applied. As the wave functions and scattering matrixes are not clear, the spectra shown here depend on specific wave function assumptions.

sidering that the diquarks are supposed under thermal distributions in current calculations and the large statistical and systematic errors of the experimental data, the value itself should not to be serious. But the fact, $\bar{\Omega}^+/\Omega^- > 1$ will remain unchanged.

6. Thermalization and Rescattering

As pointed above, the thermalization for final hadrons are omitted from all of the calculations. Considering the interactions not inserted in our treatments, some of the dominant hadrons would be partially "thermalized" effectively.

The thermalization (τ_{lax}) contains two main contributions, hadron-parton elastic cross sections and hadron (in)elastic rescattering. The elastic process may be uni-

versal for all hadrons approximately, while the contributions of inelastic rescattering for some specific hadrons are much larger than the others.

Comparing to the RHIC data, the productions of π , K , p and Λ may be well thermalized. The productions of Ω may be not. Inelastic rescattering could also regenerate some $\Sigma^*(1385)$, which may deliver strange quarks from K to $\Lambda(\Sigma)$ as a one-way valve.

The rescattering will change the spectra at low p_T . Thus, the data for K and Λ will benefit from it. The experimental data could be well satisfied by tuning τ_{lax} . While, it is not easy to tell how strong the intensity of the rescattering is, due to the large amount of uncertainties and simplifications of the model.

B. HBT Radii

Information of HBT radii will be qualitatively discussed in this subsection. The hydro models always involve in some difficulties in pion interferometry. R_{Long} and R_{Out} are too large, R_{Side} is too small. The large R_{Long} is due to the long hydrodynamic duration, the large R_{Out} is due to the transverse flow.

As mentioned above, the direct production of pion is less than 5%. The majority of pions are decay products. These large amount of decay products would form a "Decay Cloud". The cloud is so heavy that expands the HBT radii by 1 or 2 fm [64]. So, the heavy cloud should also contribute the elastic rescattering [65]. In our case, the cloud are not only composed of hadrons but also composed of SQGP droplets.

As HBT radii are not the main subject of this article, detailed calculation will not be applied here. Only some qualitatively approximations would be presented to show such ideas, that when decay expands the radius, the rescattering would make it shrink.

The hydrodynamic duration of transport hadronization is about $8.4 fm/c$. When the initial time $\tau_0 = 0.6 fm/c$ is added, the total duration is about $9 fm/c$.

For simplification, the bulk is divided to two parts [66], the emission core and the layer of decay cloud.

The survival chance for a pion passing through such cloud is described as,

$$g = e^{-\beta t}, \quad (42)$$

where,

$$\beta = \frac{c_0 + c_1 v + c_2 v^2 + \dots}{L_{elastic}}.$$

In our case,

$$\beta \approx \frac{1 + \frac{v^2}{3}}{L_{elastic}}.$$

Thus, the corrected distribution after several collisions is,

$$f' = \lim_{i \rightarrow \infty} (\alpha_0 + \alpha_1 + \alpha_2 \dots), \quad (43)$$

where α_i is the final distribution for the hadrons, which have collided i times before escaping.

$$\begin{aligned} \alpha_i \approx & \int \dots \int f_0(\mathbf{r}_0, \mathbf{p}_0) f(\mathbf{r}_1, \mathbf{p}_1) \dots f(\mathbf{r}_i, \mathbf{p}_i) \\ & \times [1 - g(\mathbf{r}_0, \mathbf{p}_0)] \dots [1 - g(\mathbf{r}_{i-1}, \mathbf{p}_{i-1})] \\ & \times g(\mathbf{r}_i, \mathbf{p}_i) d\mathbf{p}_0 \dots d\mathbf{p}_{i-1}. \end{aligned}$$

If the new distribution after each collision is assumed same and to contain no memories of their momentums, the expression can be simplified. Setting

$$\alpha_i \approx f_0 g \alpha'_i,$$

one may rewrite Eq. (43) through the method similar to the Random Phase Approximation (RPA) in NJL models [67][68],

$$f' = f_0 g \cdot \left(\frac{1}{1 - \alpha'_1} \right). \quad (44)$$

The term $\frac{1}{1 - \alpha'_1}$ provides a normalization factor, which could be omitted from HBT calculations. The factor also affected the hadron invariant production spectra, the effect as thermalization is neglected.

The HBT radii can be extracted by the method in [69][6],

$$\begin{aligned} R_{Side}^2(p) &= \langle \tilde{x}_s^2 \rangle, \\ R_{Out}^2(p) &= \langle \tilde{x}_o^2 \rangle - 2\beta_T \langle \tilde{x}_o \tilde{t} \rangle + \beta_T^2 \langle \tilde{t}^2 \rangle, \\ R_{Long}^2(p) &= \langle \tilde{z}^2 \rangle, \end{aligned}$$

where $\tilde{x}_\mu = x_\mu - \langle x_\mu \rangle$, β_T is the pair velocity.

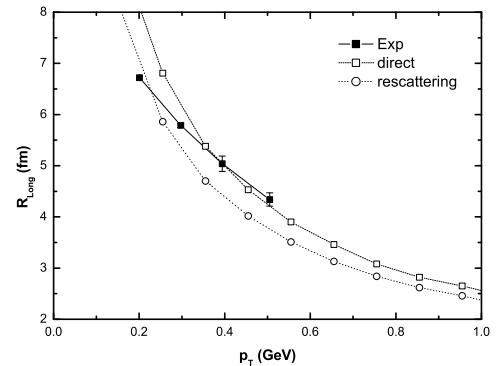


FIG. 30: Demonstration of rescattering effect on R_{Long} of π^+ interferometry at 200 GeV . $L_{elastic} = 1.5 fm$, "cloud" depth 3 fm . The layer shrinks synchronically with the hadronization surface.

Demonstrations of the rescattering effects of "decay cloud" are shown in Fig. 30 - Fig. 32 compared with STAR data [70]. The decay enhancement on HBT radii involves in detailed transport process. They are not counted in the figures. As the estimations are extremely

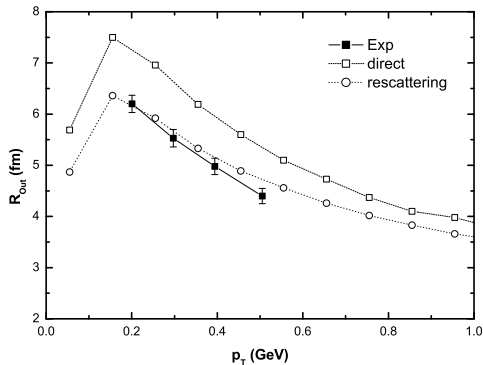


FIG. 31: Demonstration of rescattering effect on R_{Out} of π^+ interferometry at 200 GeV.

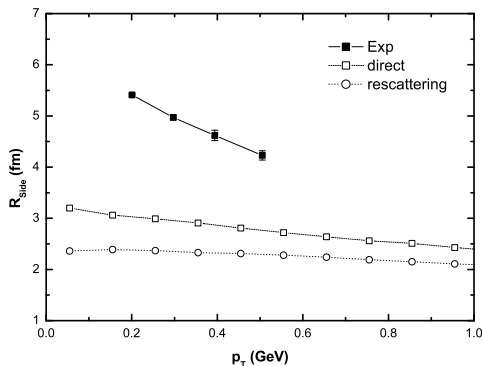


FIG. 32: Demonstration of rescattering effect on R_{Side} of π^+ interferometry at 200 GeV.

simplified, the results just show some qualitative tendency. Mean (effective) decoupling surfaces are used to provide the positions of the emitting hadrons. The surface is a kind of average for the hadron production spectra. However, the effects of the hadron interferometry can not be averaged in the same degree easily. Additionally, the decoupling droplets are supposed emit hadrons under the same distributions as in the mean decoupling surface. The position are supposed simply to be the same in the calculations for the hadron interferometry, which in fact depends on the position significantly. Thus, the picture of SQGP droplets may result to some complicated calculations [71]. Although the estimations can not satisfy the measurements well, it may provide a helpful method to resolve the HBT puzzle.

V. DISCUSSION AND OUTLOOK

A transport hadronization model is developed to describe the dynamical phase transition in the relativistic

heavy ion collisions. The SQGP fluid evolves under the hydrodynamics, and the hadrons are created by detailed SQGP production process and transport. The hadron transport results to a kind of equivalent evaporation. Based on the evaporation boundary conditions, simplified hydrodynamics with low viscosity can be applied to the SQGP medium, which is created in the collisions. The medium would split to droplets due to the hydrodynamical expansion and hadron emissions. Thus, final hadron spectra of soft production could be deduced from this model as a preliminary application. The majority of the data can be explained with some global parameters.

It is the advantage of this model that the spectra of the unthermalized heavy resonances with different masses and spin structures could be calculated naturally. The results for pions and protons is similar to those of the statistical models, because the decay contributions are equivalent to the thermalizations. But for heavier resonances, the decay contributions become smaller. The deflections from statistical distributions are remarkable. Furthermore, the in-transport decay in the medium could be deduced naturally too. Spectra, such as $K^*(892)$ could be described quite well in this way. As current quarks and diquarks are used, it is not needed to explain how constituent quarks come from the plasma. The calculations are also consistent to the earlier predictions of $\bar{\Omega}^+/\Omega^- > 1$ [19].

The spectra are dominated by decay products, thus the intensity interferometry of the system should contain the influences of hadron decay products and their interactions [64][65]. It might be a helpful solution to explain the π interferometry data, if the contributions of this two parts are considered. Current calculation can not resolve it yet, but it may be a hopeful direction deserving further studies.

The model also suffers from some disadvantages in this stage. The partons are supposed to be under thermal distributions. This situation may suppress the low p_T strange baryons. The thermal distribution for strange quarks may cause similar problems. The strange quark distribution may be overestimated. The effect is similar to the γ_s in statistical models [3]. Approximate effective lagrangians, uncertain baryon wave functions and incomplete decay properties would also make troubles.

Another one is about the approximation of evaporation. In the later stage, the whole bulk becomes loosen and consists in droplets in the whole region. The border will become diffused, the transparency will increase. The emission distribution will also be more complicated, involved with the fluid evolutions and integrations of time retardation.

The splitting of the bulk may not be a random process, even for homogeneous issues. Partons with similar momentum may tend to bind together to form a multi-quark color singlet state. Unsteady multi-quark states would decay to smaller multi-quark states or hadrons in sequence. The model may be invalid for such a different mechanism.

In any case, the model deserves more improvements in future stage. Transport of diquarks needs to be applied. Better effective lagrangians should be inserted. More over, the calculation should be upgraded to provide elliptic flows. Models using hydrodynamics results similar in low p_T invariant production spectra. More details would be extracted from v_2 data. The possible two slopes for some the the RHIC data need to pay further attentions.

Acknowledgements

We are grateful to Wojciech Broniowski, Rudolph C. Rwa, Qubing Xie, Nu Xu and Weining Zhang for useful discussions and Yuxin Liu for the careful reading of this manuscript. Special thanks to Huanzhong Huang for the lectures on RHIC experiments. This work was supported in part by the National Natural Science Foundation of China 10547001 and 10428510.

APPENDIX A: REWRITING THE BARYON WAVE FUNCTIONS

The SU(6) baryon wave functions could be rewritten in quark-diquark model [72][73]. The $(\frac{1}{2})^+$ and $(\frac{3}{2})^+$ S-wave intermediate baryon states composed of quark and diquark are introduced as,

$$\begin{aligned} B_{\frac{1}{2},+\frac{1}{2}}(A,q) &= \frac{1}{\sqrt{3}} \left(\sqrt{2}A_+q^\downarrow - A_0q^\uparrow \right), \\ B_{\frac{1}{2},+\frac{1}{2}}(S,q) &= Sq^\uparrow, \\ B_{\frac{3}{2},+\frac{3}{2}}(A,q) &= A_+q^\uparrow, \\ B_{\frac{3}{2},+\frac{1}{2}}(A,q) &= \frac{1}{\sqrt{3}} \left(A_+q^\downarrow + \sqrt{2}A_0q^\uparrow \right), \end{aligned}$$

where S represent a scalar diquark state and A represent an axial-vector diquark state. Therefore, the final baryon states can be expressed as certain combinations of these intermediate baryon states[23][19]. The SU(3) octet baryons is written as,

$$\begin{aligned} |p\rangle &= \frac{1}{\sqrt{3}} [B_{\frac{1}{2}}(A_{uu},d) - \sqrt{\frac{1}{2}}B_{\frac{1}{2}}(A_{ud},u) \\ &\quad + \sqrt{\frac{3}{2}}B_{\frac{1}{2}}(S_{ud},u)], \\ |n\rangle &= \frac{1}{\sqrt{3}} [-B_{\frac{1}{2}}(A_{dd},u) + \sqrt{\frac{1}{2}}B_{\frac{1}{2}}(A_{ud},d) \\ &\quad + \sqrt{\frac{3}{2}}B_{\frac{1}{2}}(S_{ud},d)], \end{aligned}$$

$$\begin{aligned} |\Lambda\rangle &= \frac{1}{\sqrt{3}} [\sqrt{\frac{3}{4}}B_{\frac{1}{2}}(A_{us},d) - \sqrt{\frac{3}{4}}B_{\frac{1}{2}}(A_{ds},u) \\ &\quad + \sqrt{\frac{1}{4}}B_{\frac{1}{2}}(S_{us},d) - \sqrt{\frac{1}{4}}B_{\frac{1}{2}}(S_{ds},u) \\ &\quad + B_{\frac{1}{2}}(S_{ud},s)], \\ |\Sigma^0\rangle &= \frac{1}{\sqrt{3}} [B_{\frac{1}{2}}(A_{ud},s) \\ &\quad - \sqrt{\frac{1}{4}}B_{\frac{1}{2}}(A_{us},d) - \sqrt{\frac{1}{4}}B_{\frac{1}{2}}(A_{ds},u) \\ &\quad + \sqrt{\frac{3}{4}}B_{\frac{1}{2}}(S_{us},d) + \sqrt{\frac{3}{4}}B_{\frac{1}{2}}(S_{ds},u)], \\ |\Sigma^+\rangle &= -\frac{1}{\sqrt{3}} [B_{\frac{1}{2}}(A_{uu},s) - \sqrt{\frac{1}{2}}B_{\frac{1}{2}}(A_{us},u) \quad (A1) \\ &\quad + \sqrt{\frac{3}{2}}B_{\frac{1}{2}}(S_{us},u)], \\ |\Sigma^-\rangle &= \frac{1}{\sqrt{3}} [B_{\frac{1}{2}}(A_{dd},s) - \sqrt{\frac{1}{2}}B_{\frac{1}{2}}(A_{ds},d) \\ &\quad + \sqrt{\frac{3}{2}}B_{\frac{1}{2}}(S_{ds},d)], \\ |\Xi^0\rangle &= \frac{1}{\sqrt{3}} [-B_{\frac{1}{2}}(A_{ss},u) + \sqrt{\frac{1}{2}}B_{\frac{1}{2}}(A_{us},s) \\ &\quad + \sqrt{\frac{3}{2}}B_{\frac{1}{2}}(S_{us},s)], \\ |\Xi^-\rangle &= \frac{1}{\sqrt{3}} [-B_{\frac{1}{2}}(A_{ss},d) + \sqrt{\frac{1}{2}}B_{\frac{1}{2}}(A_{ds},s) \\ &\quad + \sqrt{\frac{3}{2}}B_{\frac{1}{2}}(S_{ds},s)]. \end{aligned}$$

For decuplet baryons,

$$\begin{aligned} |\Delta^{++}\rangle &= B_{\frac{3}{2}}(A_{uu},u), \\ |\Delta^+\rangle &= \frac{1}{\sqrt{3}} [B_{\frac{3}{2}}(A_{uu},d) + \sqrt{2}B_{\frac{3}{2}}(A_{ud},u)], \\ |\Delta^0\rangle &= \frac{1}{\sqrt{3}} [B_{\frac{3}{2}}(A_{dd},u) + \sqrt{2}B_{\frac{3}{2}}(A_{ud},d)], \\ |\Delta^-\rangle &= B_{\frac{3}{2}}(A_{dd},d), \\ |\Sigma^{*+}\rangle &= \frac{1}{\sqrt{3}} [B_{\frac{3}{2}}(A_{uu},s) + \sqrt{2}B_{\frac{3}{2}}(A_{us},u)], \quad (A2) \\ |\Sigma^{*0}\rangle &= \frac{1}{\sqrt{3}} [B_{\frac{3}{2}}(A_{us},d) + B_{\frac{3}{2}}(A_{ds},u) + B_{\frac{3}{2}}(A_{ud},s)], \\ |\Sigma^{*-}\rangle &= \frac{1}{\sqrt{3}} [B_{\frac{3}{2}}(A_{dd},s) + \sqrt{2}B_{\frac{3}{2}}(A_{ds},d)], \\ |\Xi^{*0}\rangle &= \frac{1}{\sqrt{3}} [B_{\frac{3}{2}}(A_{ss},u) + \sqrt{2}B_{\frac{3}{2}}(A_{us},s)], \\ |\Xi^{*-}\rangle &= \frac{1}{\sqrt{3}} [B_{\frac{3}{2}}(A_{ss},d) + \sqrt{2}B_{\frac{3}{2}}(A_{ds},s)], \\ |\Omega^-\rangle &= B_{\frac{3}{2}}(A_{ss},s). \end{aligned}$$

From these expressions, one could get the factor C_{cg}^{ch} in Eq. (34) and (36) to complete the production rate.

It is also noted that, for the completeness of Eqs. (A2) and Eqs. (A2), there might be other orthogonal baryon states produced from QGP together with the above baryons. From the *Tables of Particle Physics* [36], $N(1440) \frac{1}{2}(\frac{1}{2}^+)$ and $N(1710) \frac{1}{2}(\frac{1}{2}^+)$ are conjectured to be the orthogonal states of p, n . Other possibilities may be, $\Lambda(1600) 0(\frac{1}{2}^+)$, $\Lambda(1810) 0(\frac{1}{2}^+)$, $\Sigma(1660) 1(\frac{1}{2}^+)$ and $\Sigma(1880) 1(\frac{1}{2}^+)$ for Λ, Σ ; $N(1720) \frac{1}{2}(\frac{3}{2}^+)$ for Δ^+, Δ^0 ; $\Lambda(1890) 0(\frac{3}{2}^+)$ and $\Sigma(1840) 1(\frac{3}{2}^+)$ for $\Sigma^*(1385)$ and some unknown states for $\Xi, \Xi^*(1530)$. There are 24 such particles, which belong to two $(\frac{1}{2})^+$ octets and a $(\frac{3}{2})^+$ octet.

The wave functions of orthogonal baryon states for $(\frac{3}{2})^+$ decuplet are determined. For example,

$$|\Lambda_2\rangle_{S=\frac{3}{2}}^{\{8\}} = \frac{1}{\sqrt{2}}[B_{\frac{3}{2}}(A_{us}, d) - B_{\frac{3}{2}}(A_{ds}, u)], \quad (A3)$$

$$|\Sigma_2^0\rangle_{S=\frac{3}{2}}^{\{8\}} = \frac{1}{\sqrt{6}}[B_{\frac{3}{2}}(A_{us}, d) + B_{\frac{3}{2}}(A_{ds}, u) - 2B_{\frac{3}{2}}(A_{ud}, s)].$$

There are two orthogonal baryon states for $(\frac{1}{2})^+$ octet. The wave functions are not unique. Considering that the first octet state is the mixed state of Aq and Sq , a most possible assumption is that the second state should be the corresponding mixed state, and the third one contains no mixing. Thus,

$$|N_2^+\rangle_{S=\frac{1}{2}}^{\{8\}} = \frac{1}{\sqrt{3}}[B_{\frac{1}{2}}(A_{uu}, d) - \sqrt{\frac{1}{2}}B_{\frac{1}{2}}(A_{ud}, u) - \sqrt{\frac{3}{2}}B_{\frac{1}{2}}(S_{ud}, u)], \quad (A4)$$

$$|N_3^+\rangle_{S=\frac{1}{2}}^{\{8\}} = \frac{1}{\sqrt{3}}[B_{\frac{1}{2}}(A_{uu}, d) + \sqrt{2}B_{\frac{1}{2}}(A_{ud}, u)].$$

Here, N_2^+ corresponds to $N(1440)^+$ and N_3^+ corresponds to $N(1710)^+$.

The wave functions of some of the $(\frac{1}{2})^-$ and $(\frac{3}{2})^-$ resonances are not clear. It is hard to distinguish a $(\frac{1}{2})^-$ or $(\frac{3}{2})^-$ state from the two candidates, $(L=1, S=\frac{1}{2})$ and $(L=1, S=\frac{3}{2})$, otherwise a mixture of them. For simplicity, all $(\frac{1}{2})^-$ baryons, except Δ , are regarded as $S=\frac{1}{2}$ octet states and all $(\frac{3}{2})^-$ baryons are regarded as $S=\frac{3}{2}$ octet or decuplet states.

Another problem is about $\Lambda(1405) 0(\frac{1}{2}^-)$ and $\Lambda(1520) 0(\frac{3}{2}^-)$. They are regarded as singlet states[36]. The quark-diquark wave functions of them are unknown. Approximately, The wave function of $\Lambda(1405)$ is also written as $S=\frac{1}{2}$ octet, $\Lambda(1520)$ as $S=\frac{3}{2}$.

APPENDIX B: EFFECTIVE LAGRANGIAN AND MATRIX ELEMENTS OF PRODUCTION CROSS SECTION

As mentioned in Section (IID), only lowest order interactions are considered. While, by the restriction of energy-momentum conservation, some of the lowest order interactions, such as two heavy components combining to one light singlet without emitting one or more gluons or photons, are forbidden. For some specific progresses, many-body final channels may play important roles. That will involve with the effective vertex of gluon and bound-state in QCD level and bring more parameters. Considering that the heavy components are scarce in amount, these contributions are not counted in so far.

Although tree level effective lagrangians are discussed, the expressions are also involved with many kinds of coupling channels and different parameters [74][75]. As there are not enough data to determine the coupling modes and constants, we have to choose some of the most simple coupling channels as the preliminary approximation. Some of the tensor-vector couplings are removed. Each lagrangian for baryon channel only contains one coupling constant g_B , which is regarded universal for all processes. There is another coupling constant g_M for mesons. The expressions in this section should NOT be regarded as the serious and final results.

As universal coupling constant is used, terms including $\partial_\mu u_q$ are avoided, which may cause divergences in some of the channels, when light current quarks are used. $q\bar{q}$ bound (resonance) states are $(\frac{1}{2})^-$ particles. The corresponding expressions of the cross section are considered equivalent to those of quarks to hadrons with opposite parity.

Meson	L_{eff}	$ M_{spin} ^2$
0^-	$ig_M \bar{q}_1 \gamma_5 q_2 \phi$	$\frac{g_M^2}{2}[m_M^2 - (m_{q1} - m_{q2})^2]$
0^+	$ig_M \bar{q}_1 q_2 \phi$	$\frac{g_M^2}{2}[m_M^2 - (m_{q1} + m_{q2})^2]$
1^-	$ig_M \bar{q}_1 \gamma_\mu q_2 \omega_\mu$	$\frac{g_M^2}{2}[m_M^2 - (m_{q1} - m_{q2})^2][\frac{(m_{q1} + m_{q2})^2}{m_M^2} + 2]$
1^+	$ig_M \bar{q}_1 \gamma_\mu \gamma_5 q_2 \omega_\mu$	$\frac{g_M^2}{2}[m_M^2 - (m_{q1} + m_{q2})^2][\frac{(m_{q1} - m_{q2})^2}{m_M^2} + 2]$
2^+	$ig_M \bar{q}_1 \gamma_\mu \gamma_\nu q_2 \kappa_{\mu\nu}$	$\frac{3g_M^2}{10}[m_M^2 - (m_{q1} + m_{q2})^2]$

TABLE IV: Expressions of $|M|^2$ for mesons.

Varies channels and effective lagrangians for mesons are listed in Tab IV. The influences of P-wave and D-wave are neglected in current stage. Formulas are arranged in $\{1, 2, 3, 4\}$ expressions.

Some of the major baryon lagrangians are discussed below approximately. For $J^P = \frac{1}{2}^+, L=0$ and $S=\frac{1}{2}$,

$$L_{qSB}^{\frac{1}{2}^+} = ig_B \bar{B} q S, \quad (B1)$$

$$L_{qAB1}^{\frac{1}{2}^+} = ig_B \bar{B} \gamma_\mu \gamma_5 q A_\mu,$$

$$|M|_{\frac{1}{2}^+}^2 = g_B^2[(m_B + m_q)^2 - m_S^2], \quad (B2)$$

$$|M|_{\frac{1}{2}^+}^2 = \frac{g_B^2}{3}[(m_B + m_q)^2 - m_A^2][\frac{(m_B - m_q)^2}{m_A^2} + 2].$$

It is noted that the forms in Eqs. (B2) are equivalent to the expressions in [19].

For $J^P = \frac{1}{2}^-$, $L = 1$ and $S = \frac{1}{2}$,

$$\begin{aligned} L_{qSB}^{\frac{1}{2}-} &= \frac{ig_B}{m_B + m_q} \bar{B} \gamma_5 \gamma_\mu q \partial_\mu S, \\ L_{qAB1}^{\frac{1}{2}-} &= \frac{ig_B}{2m_A} \bar{B} \sigma_{\mu\nu} q \partial_\nu A_\mu, \end{aligned} \quad (\text{B3})$$

where

$$\sigma_{\mu\nu} = -\frac{i}{2} [\gamma_\mu, \gamma_\nu].$$

The expression of L_{qSB} here gives the same result as direct coupling[76]. Then,

$$\begin{aligned} |M|_{\frac{1}{2}-}^2 &= g_B^2 [(m_B - m_q)^2 - m_S^2], \\ |M|_{\frac{1}{2}A1}^2 &= \frac{g_B^2}{6} [(m_B - m_q)^2 - m_A^2] \left[\frac{(m_B + m_q)^2}{m_A^2} + \frac{1}{2} \right]. \end{aligned} \quad (\text{B4})$$

For $J^P = \frac{1}{2}^-$, $L = 1$ and $S = \frac{3}{2}$, calculations are supposed to be under the the expression above for simplification.

For $J^P = \frac{3}{2}^+$ [77], $L = 0$ and $S = \frac{3}{2}$,

$$L_{qAB3}^{\frac{3}{2}+} = ig_B \bar{B}_\mu \gamma_5 q A_\mu, \quad (\text{B5})$$

$$\begin{aligned} |M|_{\frac{3}{2}A3}^2 &= \frac{g_B^2}{18} [(m_B - m_q)^2 - m_A^2] \\ &\times \left[\frac{(m_B^2 + m_A^2 - m_q^2)^2}{m_B^2 m_A^2} + 8 \right]. \end{aligned} \quad (\text{B6})$$

For $J^P = \frac{3}{2}^-$, $L = 1$ and $S = \frac{1}{2}$,

$$L_{qSB}^{\frac{3}{2}-} = \frac{ig_B}{m_S} \bar{B}_\mu \gamma_5 q \partial_\mu S, \quad (\text{B7})$$

$$\begin{aligned} |M|_{\frac{3}{2}S}^2 &= \frac{g_B^2}{6} [(m_B - m_q)^2 - m_S^2] \\ &\times \left[\frac{(m_B^2 + m_S^2 - m_q^2)^2}{m_B^2 m_S^2} - 4 \right]. \end{aligned} \quad (\text{B8})$$

The axial-vector couplings are replaced by,

$$\begin{aligned} |M|_{\frac{3}{2}A1}^2 &= \frac{g_B^2}{18} [(m_B + m_q)^2 - m_A^2] \\ &\times \left[\frac{(m_B^2 + m_A^2 - m_q^2)^2}{m_B^2 m_A^2} + 8 \right]. \end{aligned} \quad (\text{B9})$$

The same expression is used in $J^P = \frac{3}{2}^-$, $L = 1$ and $S = \frac{3}{2}$.

For $J^P = \frac{5}{2}^-$, $L = 1$ and $S = \frac{3}{2}$,

$$L_{qAB3}^{\frac{5}{2}-} = \frac{ig_B}{m_A} \bar{B}_{\mu\nu} q \partial_\mu A_\nu, \quad (\text{B10})$$

$$\begin{aligned} |M|_{\frac{5}{2}A3}^2 &= \frac{g_B^2}{48} [(m_B + m_q)^2 - m_A^2] \\ &\times \left[\frac{(m_B^2 + m_A^2 - m_q^2)^2}{m_B^2 m_A^2} - 4 \right] \left[\frac{(m_B^2 + m_A^2 - m_q^2)^2}{m_B^2 m_A^2} + 5.6 \right]. \end{aligned} \quad (\text{B11})$$

Where the expressions of spin- $\frac{5}{2}$ projector could be find in [78].

For $J^P = \frac{5}{2}^+$, $L = 2$ and $S = \frac{1}{2}$,

$$L_{qSB}^{\frac{5}{2}+} = \frac{ig_B}{m_S^2} \bar{B}_{\mu\nu} q \partial_\mu \partial_\nu S, \quad (\text{B12})$$

$$\begin{aligned} |M|_{\frac{5}{2}S}^2 &= \frac{g_B^2}{16} [(m_B + m_q)^2 - m_S^2] \\ &\times \left[\frac{(m_B^2 + m_S^2 - m_q^2)^2}{m_B^2 m_S^2} - 4 \right]^2. \end{aligned} \quad (\text{B13})$$

-
- [1] U. W. Heinz, Nucl. Phys. **A685**, 414-431 (2001), hep-ph/0009170
 - [2] J. Stachel, Nucl. Phys. **A654**, 119c-135c (1999), nucl-ex/9903007.
 - [3] J. Rafelski and J. Letessier, Phys. Lett. **B469**, 12 (1999), nucl-th/9908024.
 - [4] P. Huovinen, Nucl. Phys. **A761**, 296-312 (2005), nucl-th/0505036.
 - [5] G. E. Brown and M. Rho, Phys. Rev. Lett. **66**, 2720-2723 (1991); G. E. Brown et al., nucl-th/0608023.
 - [6] P. F. Kolb and U. W. Heinz, Invited review for 'Quark Gluon Plasma 3', Editors: R. C. Hwa and X. N. Wang, World Scientific, Singapore, nucl-th/0305084.
 - [7] W. Florkowski, W. Broniowski and A. Baran, J. Phys. **G31**, S1087-S1090 (2005), nucl-th/0412077.
 - [8] C. Nonaka and S. A. Bass, nucl-th/0607018.
 - [9] T. S. Biró and J. Zimányi, Phys. Lett. **B113**, 6 (1982); Nucl. Phys. **A395**, 525 (1983);
 - [10] T. S. Biró, P. Levai and J. Zimányi, J. Phys. **G28**, 1561-1566 (2002), hep-ph/0112137.
 - [11] R. J. Fries, J. Phys. **G30**, S853-S860 (2004), nucl-th/0403036;
 - [12] R. C. Hwa and C. B. Yang, nucl-th/0602024.
 - [13] M. Gyulassy, P. Levai and I. Vitev, Phys. Rev. Lett. **85**, 5535-5538 (2000), nucl-th/0005032; M. Gyulassy, P. Levai and I. Vitev, Nucl. Phys. **B594**, 371-419 (2001), nucl-th/0006010.
 - [14] Q. Wang and X. N. Wang, Phys. Rev. **C71**, 014903 (2005), nucl-th/0410049.
 - [15] L. G. Moretto et al., Phys. Rev. Lett. **94**, 202701 (2005), nucl-th/0412070.
 - [16] J. Adams et al., the STAR Collaboration, Phys. Rev. **C71**, 044906 (2005), nucl-ex/0411036.
 - [17] J. Rafelski and J. Letessier, Eur. Phys. J. **A29**, 107-111 (2006), nucl-th/0511016.
 - [18] P. F. Kolb and R. Rapp, Phys. Rev. **C67**, 044903 (2003),

- hep-ph/0210222.
- [19] H. Miao and C. S. Gao, J. Phys. **G31**, 179-184 (2005), hep-ph/0404037.
 - [20] H. Stocker et al., Phys. Lett. **B95**, 192-197 (1980).
 - [21] G. Bertsch et al., Phys. Rev. **D37**, 1202-1209 (1988).
 - [22] W. H. Barz, B. L. Friman, J. Knoll and H. Schulz, Phys. Lett. **B242**, 328-333 (1990).
 - [23] H. Miao, Z. B. Ma and C. S. Gao, J. Phys. **G29**, 2187-2192 (2003), hep-ph/0303164.
 - [24] E. V. Shuryak and I. Zahed, Phys. Rev. **D70**, 054507 (2004), hep-ph/0403127.
 - [25] M. Huang, P. F. Zhuang and W. Q. Chao, Phys. Rev. **D67**, 065015 (2003), hep-ph/0207008.
 - [26] S. K. Karn, hep-ph/0510239.
 - [27] I. Giannakis, D. F. Hou, J. R. Li and H. C. Ren, hep-ph/0610092.
 - [28] M. Asakawa, S. A. Bass and B. Müller, Phys. Rev. Lett. **96**, 252301 (2006), hep-ph/0603092.
 - [29] I. Arsene et al., Nucl. Phys. **A757**, 1 (2005); B. B. Back et al., Nucl. Phys. **A757**, 28 (2005); J. Adams et al., Nucl. Phys. **A757**, 102 (2005); K. Adcox et al., Nucl. Phys. **A757**, 184 (2005).
 - [30] D. H. Rischke, S. Bernard, and J. A. Maruhn, Nucl. Phys. **A595**, 346 (1995); D. H. Rischke, Y. Pürsün, and J. A. Maruhn, Nucl. Phys. **A595**, 383 (1995).
 - [31] S. Calogero, J. Math. Phys. **45**, 4042-4052 (2004), math-ph/0404043
 - [32] L. Yan, P. F. Zhuang and N. Xu, Phys. Rev. Lett. **97**, 232301 (2006), nucl-th/0608010.
 - [33] J. W. Clark, J. Cleymans and J. Rafelski, Phys. Rev. **C33**, 703 (1986).
 - [34] H. Miao, C. S. Gao and P. F. Zhuang, Commun. Theor. Phys. **46**, 1040-1046 (2006), hep-ph/0511245.
 - [35] C. S. Gao, in JingShin Theoretical Physics Symposium in Honor of Professor Ta-You Wu, edited by J. P. Hsu and L. Hsu, (World Scientific, 1998) 362.
 - [36] W. M. Yao et al., (Particle Data Group), J. Phys. **G33**, 1 (2006);
 - [37] F. Cooper and G. Frye, Phys. Rev. **D10**, 186 (1974).
 - [38] K. A. Bugaev, Phys. Rev. Lett. **90**, 252301 (2003), nucl-th/0210087.
 - [39] D. B. Lichtenberg, W. Namgung, J. G. Wills and E. Predazzi, Z. Phys. **C19**, 19 (1983); D. B. Lichtenberg, R. Roncaglia and E. Predazzi, hep-ph/9611428.
 - [40] J. P. Boris, D. L. Book, J. Comp. Phys. **11**, 38 (1973); J. P. Boris, D. L. Book, and K. Hain, J. Comp. Phys. **18**, 248 (1995).
 - [41] H. Miao, Z. B. Ma and C. S. Gao, Commun. Theor. Phys. **38**, 698-702 (2002), hep-ph/0303134.
 - [42] A. Bialas, M. Bleszynski and W. Czyz, Nucl. Phys. **B111**, 461 (1976).
 - [43] S. S. Adler et al, the PHENIX Collaboration, Phys. Rev. **C69**, 034909 (2004), nucl-ex/0307022.
 - [44] B. B. Back et al., the PHOBOS Collaboration, Phys. Rev. **C70**, 051901(R) (2004), nucl-ex/0401006.
 - [45] B. I. Abelev et al, the STAR Collaboration, Phys. Rev. Lett. **97**, 152301 (2006), nucl-ex/0606003.
 - [46] M. Estienne (for the STAR Collaboration), J. Phys. **G31**, S873-S880 (2005), nucl-ex/0412041.
 - [47] J. Adams et al., the STAR Collaboration, nucl-ex/0606014.
 - [48] J. Adams et al., the STAR Collaboration, nucl-ex/0601042.
 - [49] J. Adams et al., the STAR Collaboration, Phys. Rev. **C71**, 064902 (2005), nucl-ex/0412019.
 - [50] J. Adams et al., the STAR Collaboration, Phys. Lett. **B612**, 181 (2005), nucl-ex/0406003.
 - [51] S. S. Adler et al, the PHENIX Collaboration, Phys. Rev. **C72**, 014903 (2005), nucl-ex/0410012.
 - [52] J. Adams et al., the STAR Collaboration, Phys. Rev. Lett. **97**, 132301 (2006), nucl-ex/0604019.
 - [53] R. Witt (for the STAR Collaboration), talks on QM2006.
 - [54] S. Salur (for the STAR Collaboration), 22nd Winter Workshop on Nuclear Dynamics Talk Proceedings, nucl-ex/0606006.
 - [55] S-L. Blyth (for the STAR Collaboration), nucl-ex/0608019.
 - [56] Z. Fodor and S. Katz, JHEP 0203, 014 (2002), hep-lat/0106002.
 - [57] F. Karsch, Nucl. Phys. (Proc Suppl) 83-84, 14 (2000).
 - [58] J. H. Chen et al, Phys. Rev. **C74**, 064902 (2006), nucl-th/0504055.
 - [59] J. Harris, Overview of First Results from Star, (for STAR Collaboration), Quark Matter 2002.
 - [60] C. Adler et al., the STAR Collaboration, Phys. Rev. Lett. **89**, 092301 (2002).
 - [61] K. Adcox et al., the PHENIX Collaboration, Phys. Rev. Lett. **89**, 092302 (2002).
 - [62] M. Bleicher et al., Phys. Rev. Lett. **88**, 202501 (2002).
 - [63] J. Zimanyi et al., Talk given at 30th International Symposium on Multiparticle Dynamics (ISMD 2000), Tihany, Lake Balaton, Hungary, 9-15 Oct 2000, hep-ph/0103156.
 - [64] A. Kisiel, W. Florkowski, W. Broniowski and J. Pluta, Phys. Rev. **C73**, 064902 (2006), nucl-th/0602039.
 - [65] J. I. Kapusta and Y. Li, Phys. Rev. **C72**, 064902 (2005), nucl-th/0503075.
 - [66] K. Werner, hep-ph/0603064.
 - [67] Y. Nambu and G. Jona-Lasinio, Phys. Rev. **122**, 345 (1961); Y. Nambu and G. Jona-Lasinio, Phys. Rev. **124**, 246 (1961).
 - [68] S. Klevansky, Rev. Mod. Phys. **64**, 649-708 (1992).
 - [69] S. Soff, S. A. Bass and A. Dumitru, Phys. Rev. Lett. **86**, 3981-3984 (2001), nucl-th/0012085.
 - [70] J. Adams et al., the STAR Collaboration, Phys. Rev. **C71**, 044906 (2005), nucl-ex/0411036.
 - [71] W. N. Zhang et al., Phys. Rev. **C71**, 064908 (2005); W. N. Zhang, Y. Y. Ren and C. Y. Wong, Phys. Rev. **C74**, 024908 (2006).
 - [72] M. I. Pavković, Phys. Rev. **D13**, 2128-2138 (1976).
 - [73] B. Q. Ma, I. Schmidt and J. J. Yang, Phys. Lett. **B477**, 107-113 (2000), hep-ph/9906424.
 - [74] G. Penner and U. Mosel, Phys. Rev. **C66**, 055211 (2002), nucl-th/0207066.
 - [75] S. L. Zhu, Phys. Rev. **C59**, 435-441 (1999), nucl-th/9809032.
 - [76] S. L. Zhu, W-Y. P. Hwang and Y. B. Dai, Phys. Rev. **C59**, 442-450 (1999), nucl-th/9809033.
 - [77] W. Rarita and J. Schwinger, Phys. Rev. **60**, 61-61 (1941).
 - [78] V. Shklyar, G. Penner and U. Mosel, hep-ph/0301152.